SUPPLEMENTARY INFORMATION

SUPPLEMENTARY FIGURES AND FIGURE LEGENDS

FIGURE S1

A

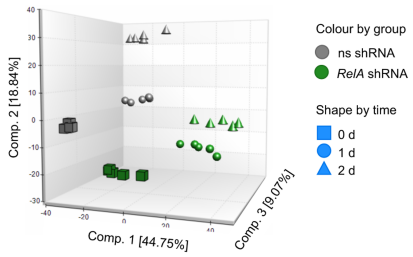

B

Platform	Time (hr)	Biochemicals q<0.05	(↑|↓)
General	0	190	97|93
	24	176	106|70
	48	257	228|29
True Mass (lipidomic)	0	598	486|112
	24	760	727|33
	48	798	722|76

C

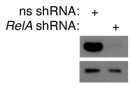

FIGURE S1, related to FIGURE 1. Disruption of cell metabolism by NF-κB inhibition during starvation

A, 3D scatter plot showing a principal component analysis (PCA) of the metabolic profile of MEFs expressing RelA-specific (RelA; green) or ns (grey) shRNAs cultured under normal conditions or for the indicated times under GL (n=5).

B, Table summarising the metabolites exhibiting differential abundance in RelA-deficient (RelA) relative to control (ns) MEFs at the indicated times after GL, according to the general metabolomic (n=488) and lipidomic (n=1028) platforms. The number of

significantly upregulated (↑) and downregulated (↓) biochemicals are depicted. Significant differences in metabolite abundance between experimental groups were identified using ANOVA contrasts (q<0.05).

C, Western blots showing the protein levels of RelA and β-actin in MEFs from (**A**).

FIGURE S2

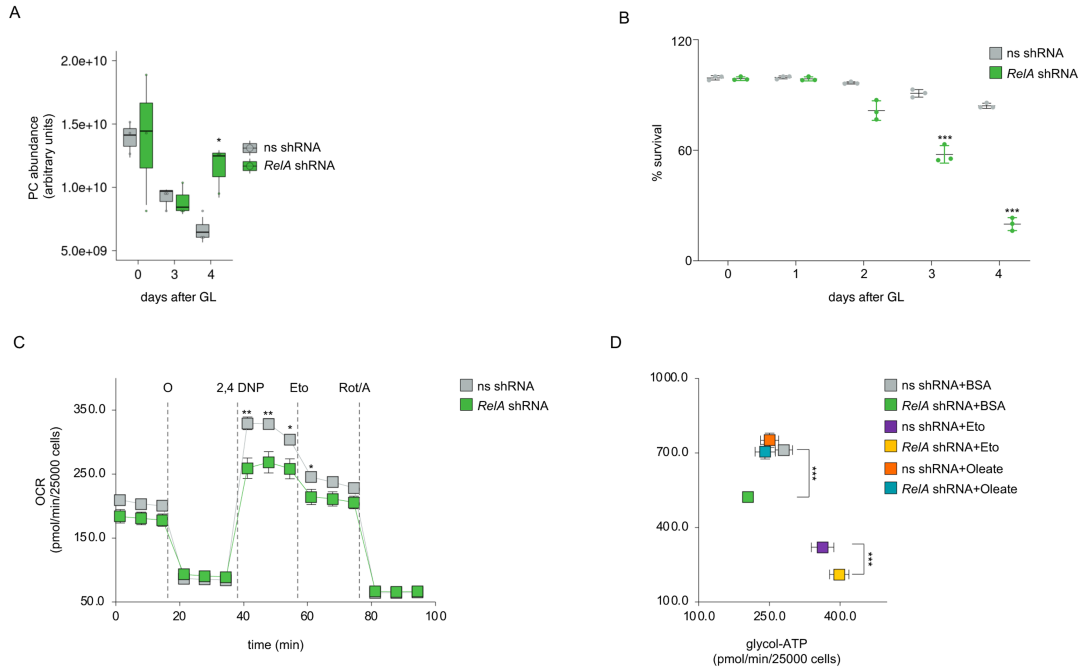

FIGURE S2, related to FIGURE 2. NF-κB inhibition impairs SRC, mitochondrial ATP production rate, and CRC cell survival during starvation

A, Boxplots showing the relative total phosphatidylcholine (PC) abundance (n=42) in CT-26 cells from Figure 2A at the indicated times after GL. The relative total PC abundance was derived by adding the peak areas of the identified PC species, determined by LC-MS following data processing using Lipostar software. Shown in the boxplots are the median values (horizontal lines), 25th-75th percentiles (box outlines),

and highest and lowest values within 1.5x of the inter-quartile range (vertical lines). *, $p<0.05$.

B, Trypan blue exclusion assays showing the percentage of live CT-26 cells from (**A**) after culture for the indicated times under GL. Values denote means ± SD (n=3). ***, $p<0.001$.

C, Oxygen consumption rate (OCR) profile measured using a Seahorse XFe96 analyser in CT-26 cells expressing RelA-specific or ns shRNAs as in (**A**), at baseline (0) and after treatment with the indicated drugs for the times shown (n=6). O, oligomycin; 2,4-DNP, 2,4-dinitrophenol; Eto, etomoxir; Rot/AA, rotenone/antimycin A.

D, Energy map showing the mitochondrial (mito-ATP) and glycolytic (glyco-ATP) ATP production rates measured using a Seahorse XFe96 analyser in CT-26 cells from Figure 2H, treated as indicated (n=8).

B-D, Statistical significance was calculated using two-tailed Student's t-test.

C-D, Values denote means ± SEM.

FIGURE S3

A

Gene Symbol	Human orthologue	Description	Function
Ces1d	***CES1***	Carboxilesterase 1d	Triacylglycerol lipase activity
Parp14	*PARP14*	Poly(ADP-Ribose) Polymerase Family Member 14	NAD^+ ADP-ribosyltransferase activity
Aoc3	*AOC3*	Amine Oxidase, Copper Containing 3	oxidoreductase activity
Fmod	*FMOD*	Fibromodulin	extracellular matrix constituent
Ogn	*OGN*	Osteoglycin	extracellular matrix constituent
Aldh6a1	*ALDH6A1*	Aldehyde Dehydrogenase 6 Family Member A1	methylmalonate-semialdehyde dehydrogenase activity
Azin2	*AZIN2*	Antizyme Inhibitor 2	arginine decarboxylase activity

B

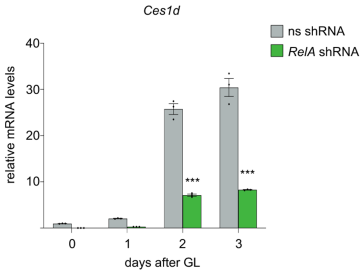

C

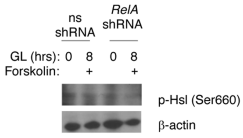

D

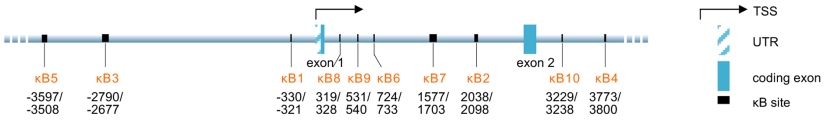

κB1 5'-gaaggacccc-3'

κB2 5'-gggtcttccctggtgtgttctttctcttccaggattacctttctctgtcctggactcctcc-3'

κB3 5'-ggaattctcttagaaattctgggaactggactggataccacatttaaattagcagctcctggacaccaagtctcagaaatcttactcaagaaaataaaatcatgggaaagacccc-3'

κB4 5'-tgaaagccccgttcaggaggaattctcc-3'

κB5 5'-gggagactctgtcagcctcaccctcaggggagcccaaatgagactactttacatggaagatgattgtggccaaggctttggggagactgc-3'

κB6 5'-tgaagctccc-3'

κB7 5'-ggagttttcagttctagtgaccacttcccactaaatttggaaatttcctgtcttttctggccacaagctttgaggaagaatgacatcttgtctaaattcaaaggccctacccaatgagggatgttct-3'

κB8 5'-gggataccca-3'

κB9 5'-gggaaccccc-3'

κB10 5'-gaagaattcc-3'

FIGURE S3

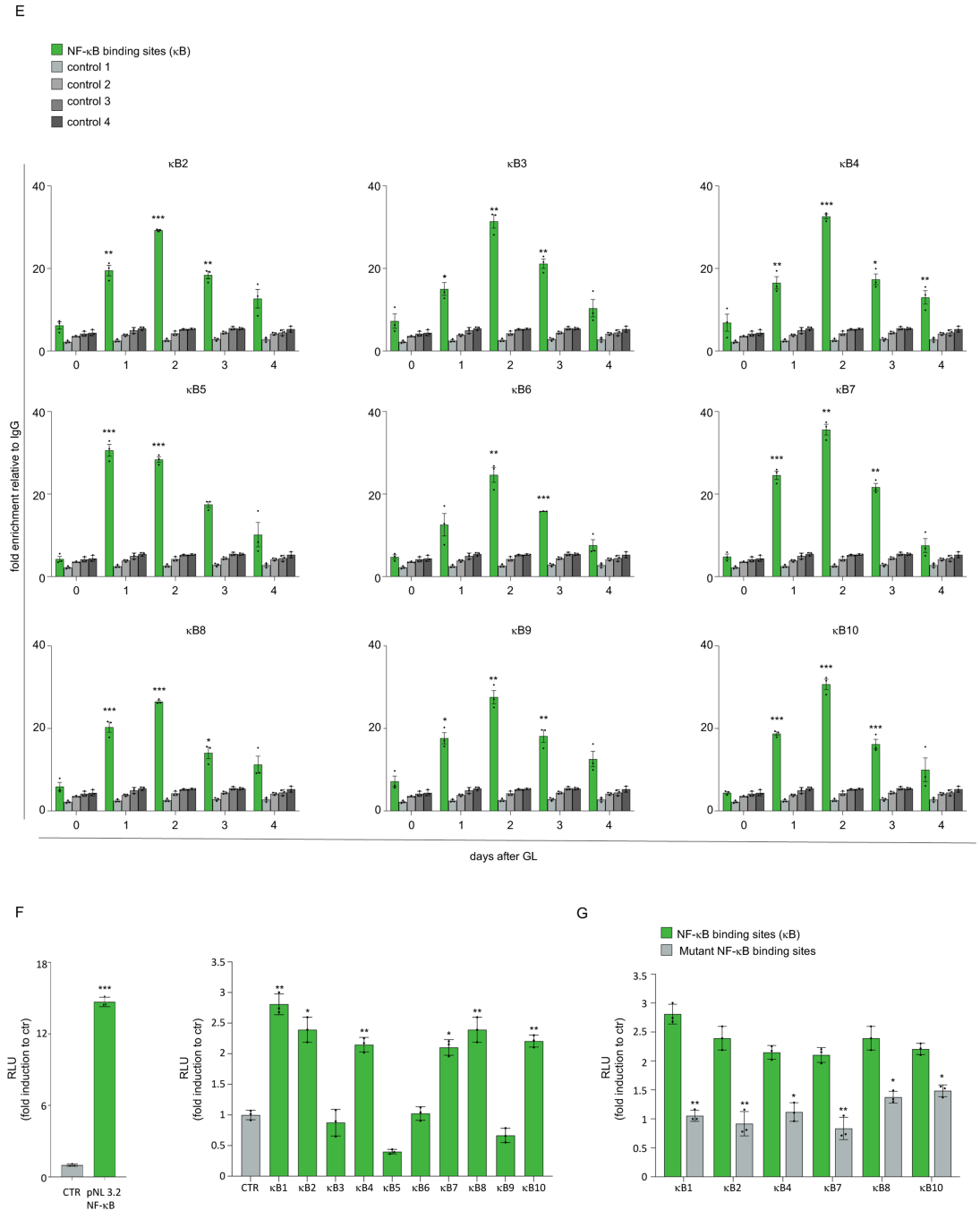

FIGURE S3, related to FIGURE 3. *Ces1d* is a direct transcriptional target of NF-κB and one of the top seven metabolic genes upregulated by NF-κB during GL

A, Table listing the seven most downregulated genes according to fold change in RelA-deficient relative to control MEFs across all time points investigated in Figure 3A.

B, qRT-PCR showing the *Ces1d* mRNA levels in MEFs expressing RelA-specific or ns shRNAs and cultured under normal conditions (0) or for the indicated times under GL. Values denote means ± SD (n=3).

C, Western blots showing β-actin and phosphorylated (p) hormone-sensitive lipase (Hsl) (Ser660) in CT-26 cells expressing RelA-specific (RelA) or non-specific (ns) shRNAs and treated with forskolin (+) or left untreated, under normal or GL conditions, as shown.

D, Schematic representation of the NF-κB-binding (κB) DNA elements identified in the *Ces1d* locus. Shown are the position relative to the transcription start site (TSS) and nucleotide sequence of each of the NF-κB-binding sites identified by chromatin immunoprecipitation in Figure 3E and Figure S3E. UTR, untranslated region.

E, Chromatin immunoprecipitation assays showing the binding of RelA-containing NF-κB complexes to the indicated κB DNA elements in the promoter and intronic regions of *Ces1d* or the indicated control DNA regions (controls 1-4) in CT-26 cells from Figure 3B. Values denote means ± SEM (n=3).

F, Dual luciferase reporter assays in HEK 293 cells cultured under GL showing the luciferase activity measured with the NF-κB-dependent positive control vector (pNL3.2-NF-κB) (left) or the vectors containing each of the NF-κB-binding sites from the *Ces1d* locus (Figure 3E, Figure S3E) (right) relative to the empty negative control vector (CTR), lacking NF-κB-binding sites. Nanoluc luciferase activity was normalized to firefly luciferase activity.

G, Dual luciferase reporter assays in HEK 293 cells cultured under GL showing the luciferase activity measured with the reporter vectors containing each of the NF-κB-binding elements from the *Ces1d* locus or the corresponding reporter vectors

containing mutated κB elements relative to the negative control vector (CTR). Nanoluc luciferase activity was normalized to firefly luciferase activity.

B, **E-G**, Statistical significance was calculated by two-tailed Student's t-test. *, $p<0.05$; **, $p<0.01$; ***, $p<0.001$.

FIGURE S4

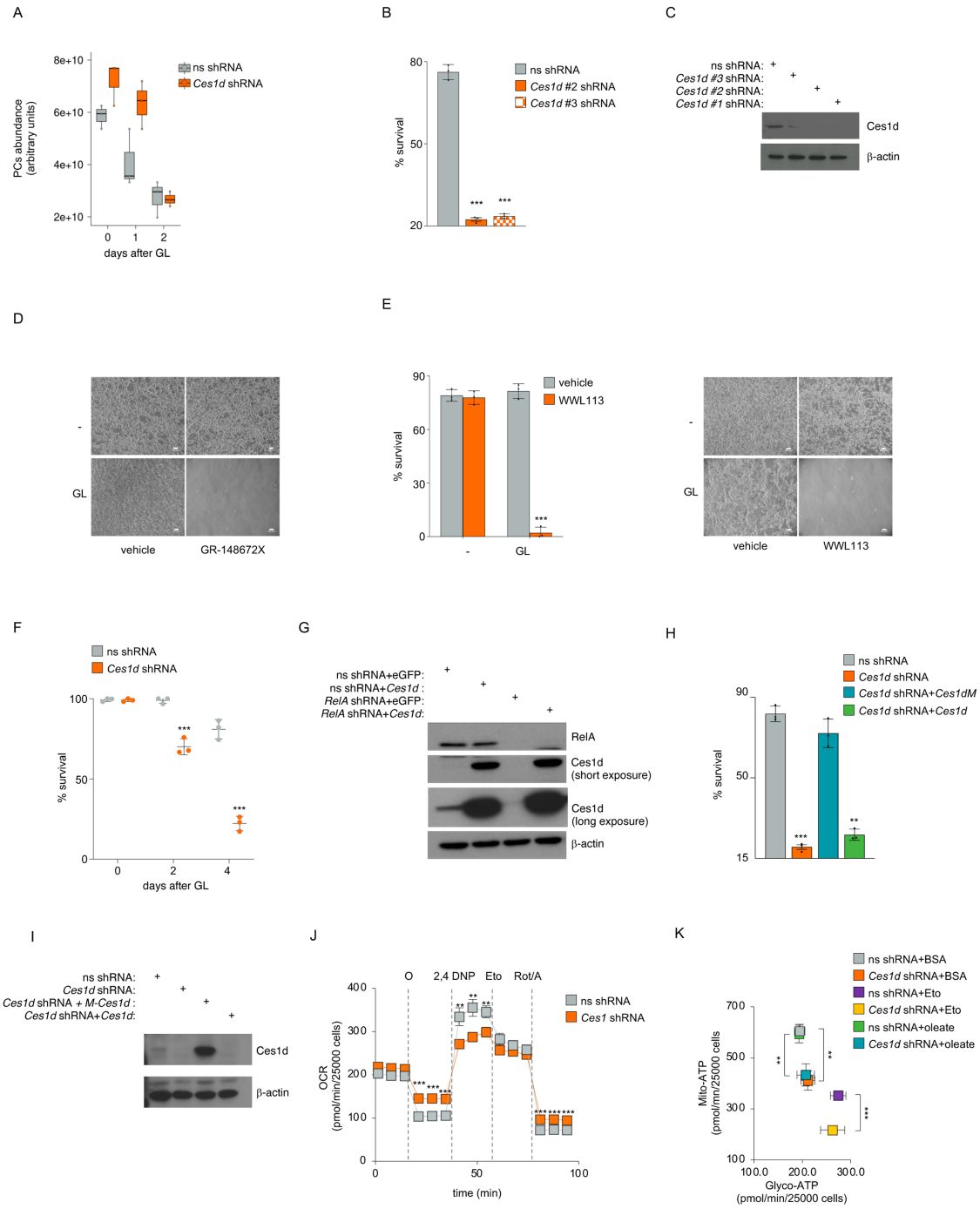
A
PCs abundance (arbitrary units)
8e+10
6e+10
4e+10
2e+10
0 1 2
days after GL
ns shRNA
Ces1d shRNA
B
% survival
80
50
20
ns shRNA
Ces1d #2 shRNA
Ces1d #3 shRNA
***
***
C
ns shRNA: +
Ces1d #3 shRNA:
Ces1d #2 shRNA: +
Ces1d #1 shRNA: +
Ces1d
β-actin
D
-
GL
vehicle
GR-148672X
E
% survival
90
60
30
0
vehicle
WWL113
***
-
GL
-
GL
vehicle
WWL113
F
ns shRNA
Ces1d shRNA
% survival
100
50
0
***
***
0 2 4
days after GL
G
ns shRNA+eGFP: +
ns shRNA+Ces1d : +
RelA shRNA+eGFP: +
RelA shRNA+Ces1d: +
RelA
Ces1d (short exposure)
Ces1d (long exposure)
β-actin
H
ns shRNA
Ces1d shRNA
Ces1d shRNA+Ces1dM
Ces1d shRNA+Ces1d
% survival
90
50
15
***
**
I
ns shRNA: +
Ces1d shRNA: +
Ces1d shRNA + M-Ces1d : +
Ces1d shRNA+Ces1d: +
Ces1d
β-actin
J
O 2,4 DNP Eto Rot/A
OCR (pmol/min/25000 cells)
400
300
200
100
0
0 50 100
time (min)
ns shRNA
Ces1 shRNA
K
ns shRNA+BSA
Ces1d shRNA+BSA
ns shRNA+Eto
Ces1d shRNA+Eto
ns shRNA+oleate
Ces1d shRNA+oleate
Mito-ATP (pmol/min/25000 cells)
700
500
300
100
100.0 200.0 300.0
Glyco-ATP (pmol/min/25000 cells)

FIGURE S4

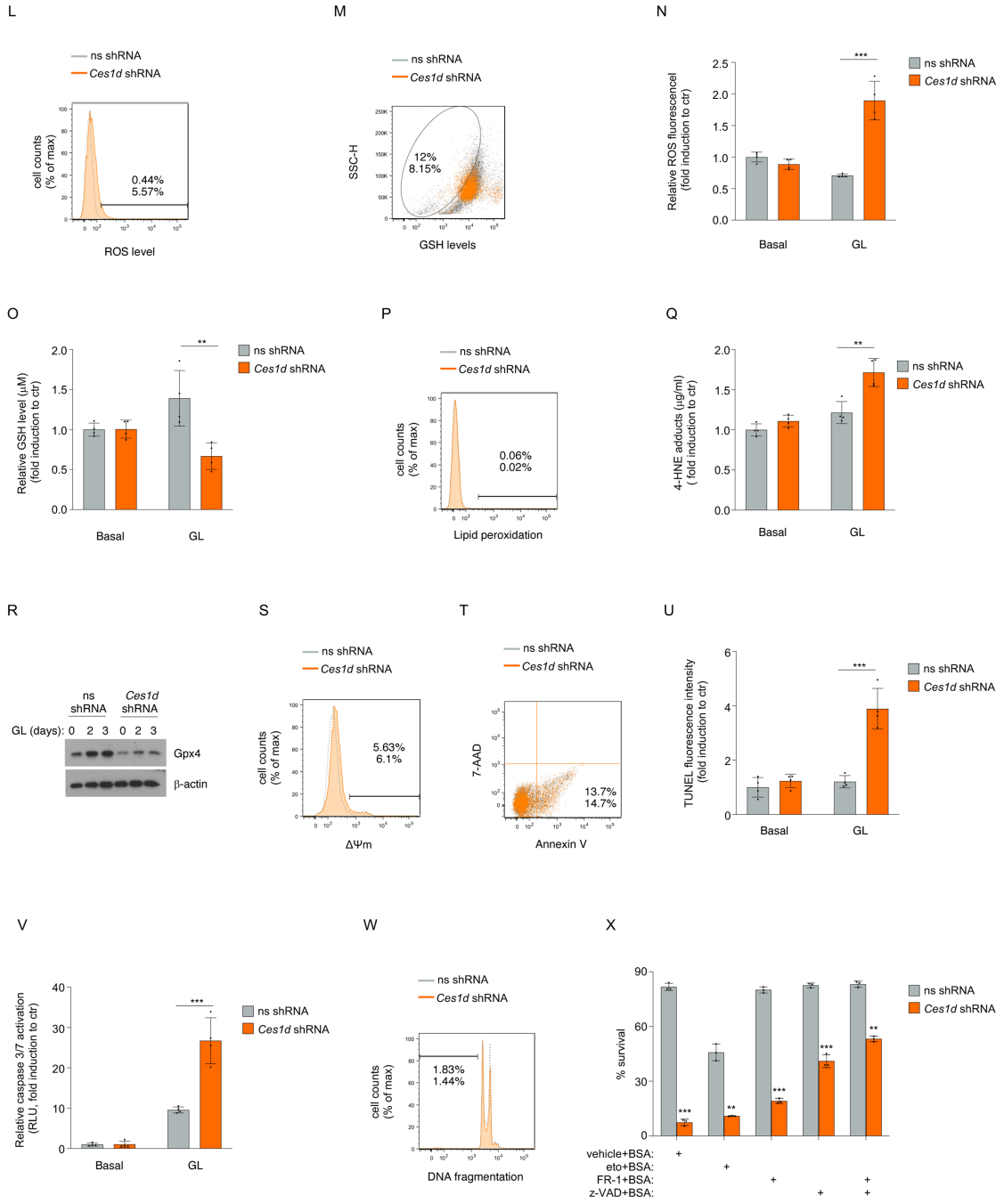

FIGURE S4, related to FIGURE 4. Ces1d mediates NF-κB-dependent metabolic adaptation by enhancing oxidative FFA catabolism and preventing toxic TAG accumulation

A, Boxplots showing the relative total PC abundance (n=55) in CT-26 cells from Figure 4A at the indicated times after GL. Relative total PC abundance was derived by adding the peak areas of the identified PC species, determined by LC-MS following data processing using Lipostar software. Shown in the boxplots are the median values (horizontal lines), 25^{th}-75^{th} percentiles (box outlines), and highest and lowest values within 1.5x of the inter-quartile range (vertical lines).

B, Trypan blue exclusion assays showing the percentage of live CT-26 cells expressing ns or the indicated additional, independent Ces1d-specific (Ces1d) shRNAs after a 4-day culture under GL.

C, Western blots showing the protein levels of Ces1d and β-actin in CT-26 cells expressing ns or the indicated Ces1d-specific (Ces1d) shRNAs.

D, Images of CT-26 cells after a 4-day treatment with GR-148672X (10 μM) or vehicle under normal culture conditions (-) or GL. Scale bar, 50 μm.

E, Trypan blue exclusion assays showing the percentage of live CT-26 cells after a 4-day treatment with WWL113 (2.5 μM) or vehicle under normal culture conditions (-) or GL (left). Images of representative cells (right). Scale bar, 50 μm.

F, Trypan blue exclusion assays showing the percentage of live MEFs expressing Ces1d-specific or ns shRNAs and cultured for the indicated times under GL.

G, Western blots showing the protein levels of RelA, Ces1d and β-actin in CT-26 cells from Figure 4G.

H, Trypan blue exclusion assays showing the percentage of live CT-26 cells expressing Ces1d-specific or ns shRNAs and infected with wild-type or RNAi-resistant (Ces1dM) Ces1d-expressing lentivirus or no Ces1-expressing lentivirus, as shown, after a 4-day culture under GL.

I, Western blots showing the protein levels of Ces1d and β-actin in CT-26 cells infected with lentivirus as in (**G**).

J, OCR profile measured using a Seahorse XFe96 analyzer in CT-26 cells expressing Ces1d-specific or ns shRNAs, at baseline (0) and after treatment with the indicated inhibitors for the times shown (n=6). O, oligomycin; 2,4-DNP, 2,4-dinitrophenol; Eto, etomoxir; Rot/AA, rotenone/antimycin A.

K, Energy map determined by using a Seahorse XFe96 analyzer and showing the mitochondrial (Mito-ATP) and glycolytic (Glyco-ATP) ATP production rates in CT-26 cells from Figure 4I (n=6).

L, FACS analysis showing ROS levels in CT-26 cells from Figure 4K, cultured under basal conditions. The percentages of cells exhibiting elevated ROS levels are depicted.

M, FACS analysis showing GSH levels in CT-26 cells from Figure 4L, cultured under basal conditions. The percentages of cells exhibiting reduced GSH levels are depicted.

N, Relative ROS levels in CT-26 cells from Figure 4A after culture under basal conditions or GL, measured by using the fluorometric DCFDA Cellular ROS Detection Assay Kit.

O, Relative GSH levels in CT-26 cells from Figure 4A after culture under basal conditions or GL, measured by using the GSH-Glo™ Glutathione Assay.

P, FACS analysis showing the levels of lipid peroxidation in CT-26 cells from Figure 4M, cultured under basal conditions. The percentages of cells exhibiting lipid peroxidation are depicted.

Q, Relative levels of 4HNE-protein-abducts in CT-26 cells from Figure 4A after culture under basal conditions or GL, measured by using the Lipid Peroxidation (4-HNE) Assay Kit.

R, Western blots showing the protein levels of Gpx4 and β-actin in CT-26 cells from Figure 4A.

S, FACS analysis showing the loss of mitochondrial membrane potential (ΔΨm) in CT-26 cells from Figure 4N, cultured under basal conditions. The percentages of cells exhibiting ΔΨm loss are depicted.

T, FACS analysis showing the percentage of CT-26 cells from Figure 4O staining positive for annexin V after culture under basal conditions. The percentages of cells staining positive for annexin V are depicted.

U, Relative nucleosomal DNA fragmentation in CT-26 cells from Figure 4A after culture under basal conditions or GL, measured by using the fluorescence-based Cell Meter™ Live Cell TUNEL Apoptosis Assay Kit.

V, Relative caspase 3/7 activity in CT-26 cells from Figure 4A after culture under basal conditions or GL, measured by using the luminescence-based Caspase-Glo® 3/7 Assay.

W, PI nuclear staining assays showing the percentage of apoptotic CT-26 cells (*i.e.*, cells exhibiting sub-G_1 DNA content) in representative cell cultures from Figure 4A under basal conditions. The percentages of apoptotic cells are depicted.

X, Trypan blue exclusion assays showing the percentage of live CT-26 cells from (**F**) after a 4-day culture under GL in the presence of the indicated treatments. Eto, etomoxir (10 μM); z-VAD, z-VAD-fmk (50 μM); FR-1, Ferrostatin-1 (0.5 μM).

B, **E-F**, **H**, **N**, **O**, **Q**, **U**, **V**, **X**, Values denote means ± SD (n=3).

J-K, Values denote means ± SEM.

A-B, **E-F**, **H**, **J-K**, **N**, **O**, **Q**, **U**, **V**, **X**, Statistical significance was calculated by two-tailed Student's t-test. **, $p<0.01$; ***, $p<0.001$.

FIGURE S5

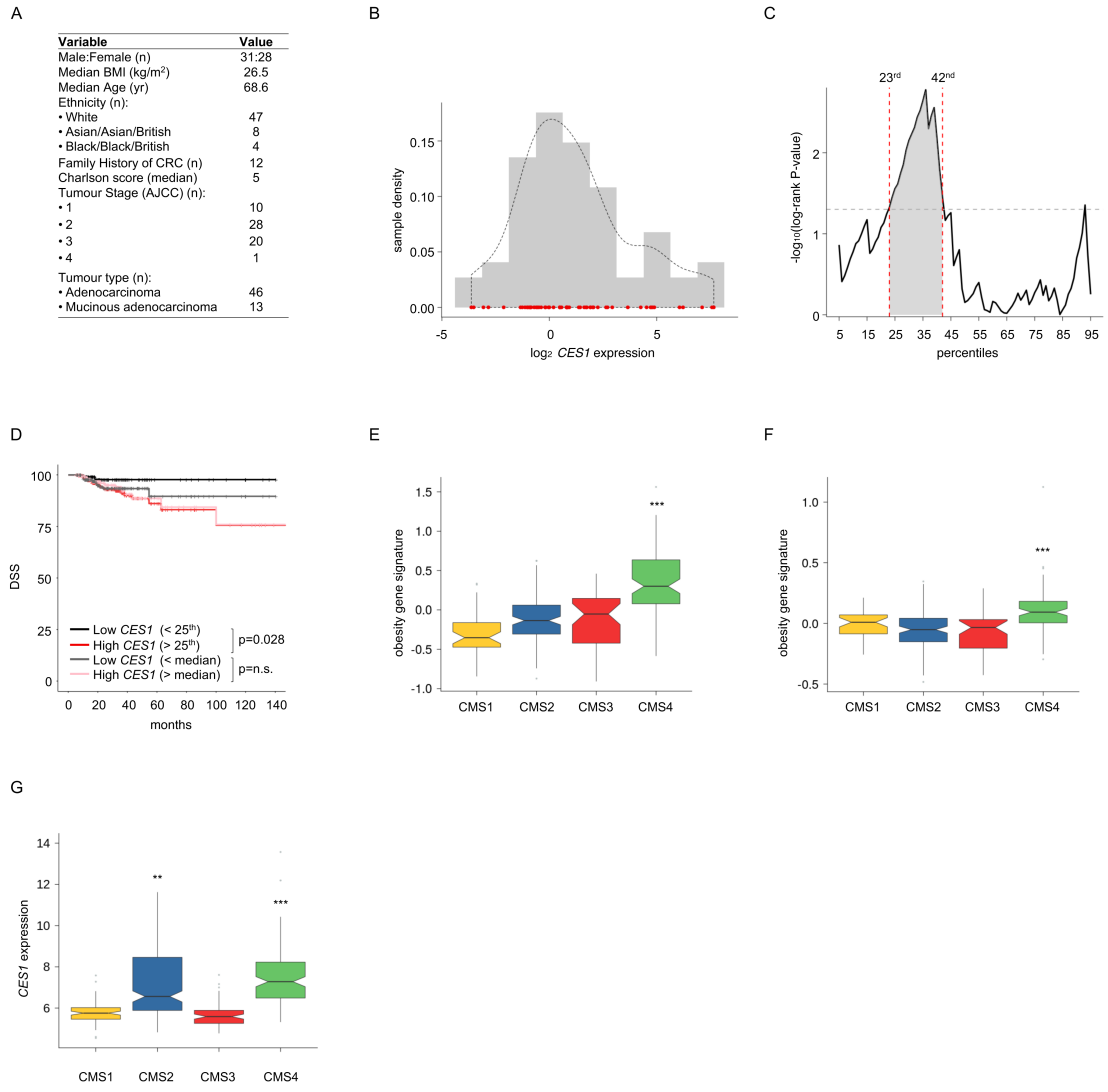

FIGURE S5

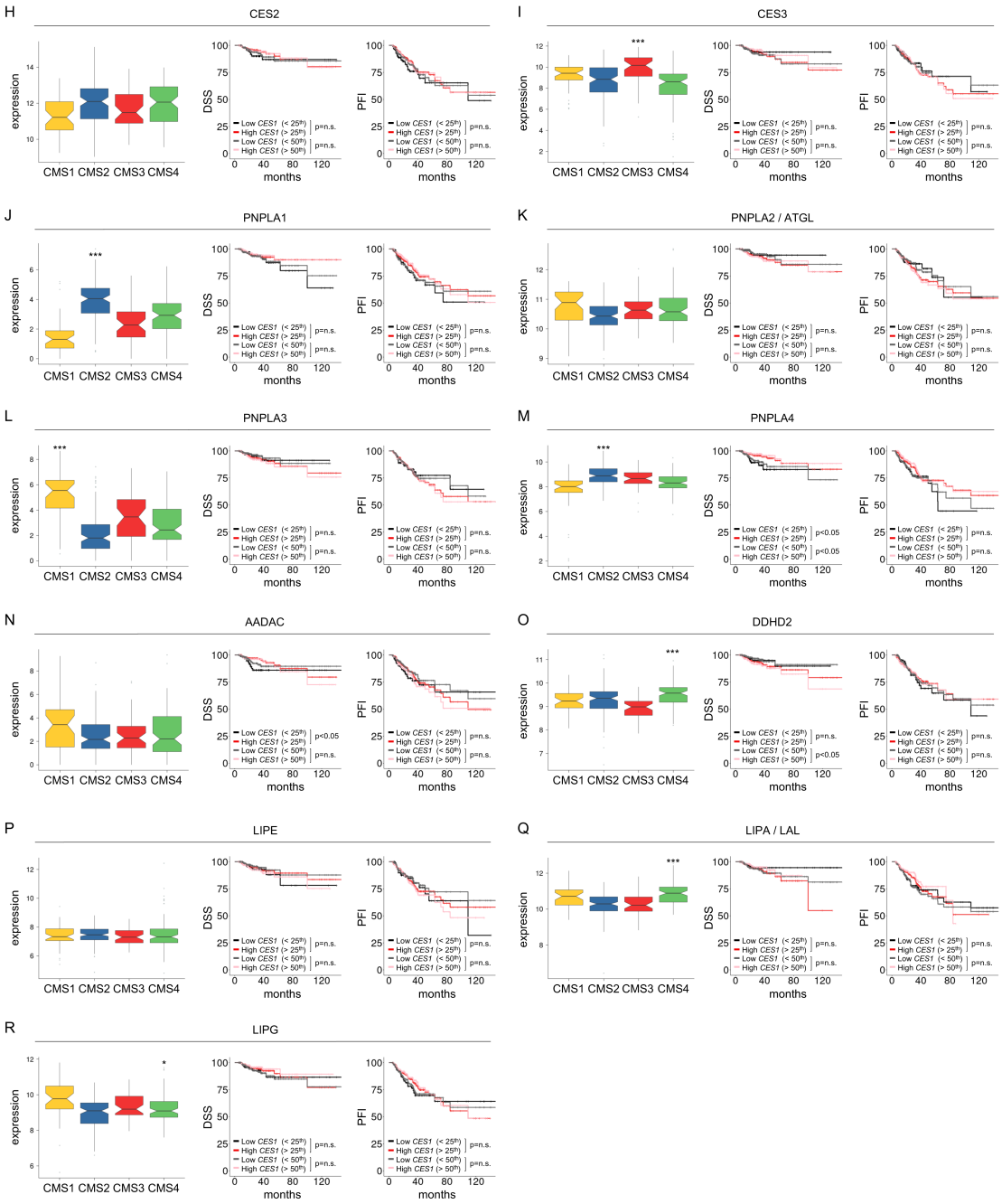
H
CES2
I
CES3
J
PNPLA1
K
PNPLA2 / ATGL
L
PNPLA3
M
PNPLA4
N
AADAC
O
DDHD2
P
LIPE
Q
LIPA / LAL
R
LIPG
expression
CMS1 CMS2 CMS3 CMS4
DSS
PFI
months
Low CES1 (< 25th)
High CES1 (> 25th)
Low CES1 (< 50th)
High CES1 (> 50th)
p=n.s.
p<0.05

FIGURE S5

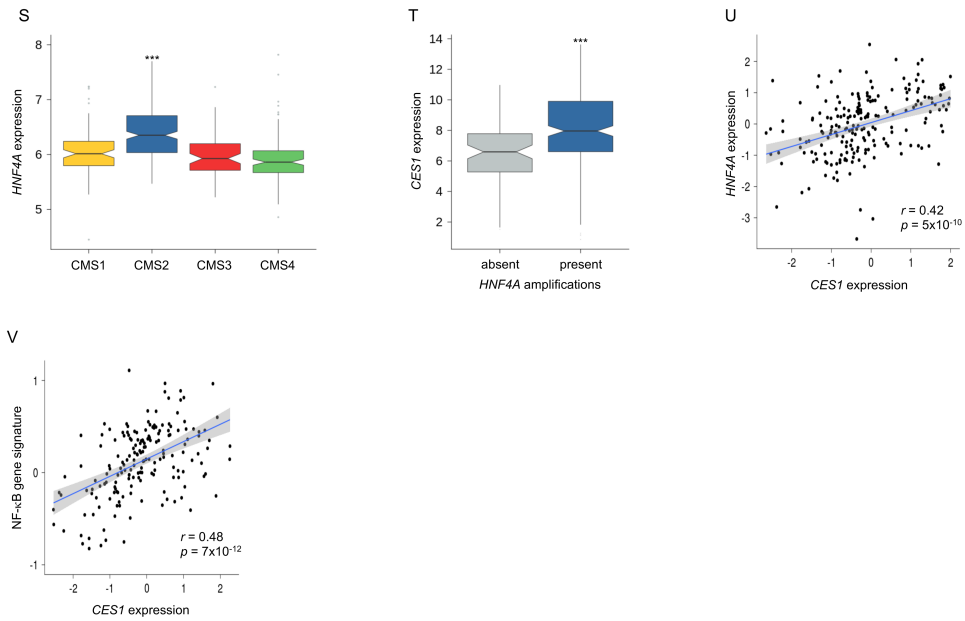

FIGURE S5, related to FIGURE 5. *CES1* is the only intracellular TAG lipase that co-distributes with the NF-κB target-gene signature and HNF4α expression in core CRC subtypes and correlates with worse prognosis in CRC patients

A, Table summarising the key demographic and clinical data from the CRC patients reported in Figure 5A-5B.

B, Histogram and sample density (dotted line) plots of CRC-associated *CES1* expression in the patients in (**A**), assessed by qRT-PCR (n=59).

C, Distribution of the log-rank p-values for the Kaplan-Meier curves generated from the TCGA dataset (n=427) when considering each percentile as a possible stratification threshold to distinguish between patients with high versus low *CES1* expression. The range of thresholds within which *CES1* expression is a statistically significant prognosticator of clinical outcome (DSS) is depicted in grey. Horizontal dotted line, p=0.05.

D, DSS in CRC patients from the TCGA dataset (n=427) stratified on the basis of tumor-associated *CES1* mRNA expression as in Figure 5A.

E, **F**, Boxplots showing the median Z-scores of two additional obesity gene signatures in each CMS CRC subtype from Figure 1A.

G, Boxplots showing the *CES1* mRNA expression in CMS CRC subtypes from patients in the French National Cartes d'identite' des Tumeurs (FNCIT) dataset (n=519). Statistical significance for multiple comparisons was calculated by using the Kruskal-Wallis test ($p<2.2x10^{-16}$).

H-R, Boxplots showing the expression of intracellular TAG lipases other than CES1 in CMS CRC subtypes from patients in the TCGA dataset (n=427) (left). DSS (middle) and PFI (right) in the same CRC patients from the TCGA dataset stratified on the basis of the tumour-associated mRNA expression of each indicated intracellular TAG lipase. Statistical significance for Kaplan-Meyer curves was calculated using the log-rank test.

S, Boxplots showing the *HNF4A* mRNA expression in CMS CRC subtypes from patients in the FNCIT dataset (n=519). Statistical significance for multiple comparisons was calculated using the Kruskal-Wallis test ($p<1x10^{-16}$).

T, Boxplots showing the *CES1* mRNA expression in CRCs exhibiting (present) or not exhibiting (absent) *HNF4A* amplifications, as indicated, in patients from the TCGA dataset (n=297). Statistical significance was calculated using two-tailed Student's t-test.

U-V, Shown are the correlations of *CES1* mRNA expression with *HNF4A* mRNA expression (**U**) and the NF-κB target-gene signature (**V**) in CRC patients from the TCGA dataset. Expression values are represented as Z-scores. Pearson's correlation values are shown.

E-S, Samples from each CMS subtype were compared to all other CRC samples using two-tailed Student's t-test. *, $p<0.05$; **, $p<0.01$; ***, $p<0.001$.

E-T, Shown in the boxplots are the median values (horizontal lines), 25^{th}-75^{th} percentiles (box outlines), and highest and lowest values within 1.5x of the inter-quartile range (vertical lines). Notches denote the 95% confidence interval of the medians. ***, $p<0.001$.

FIGURE S6

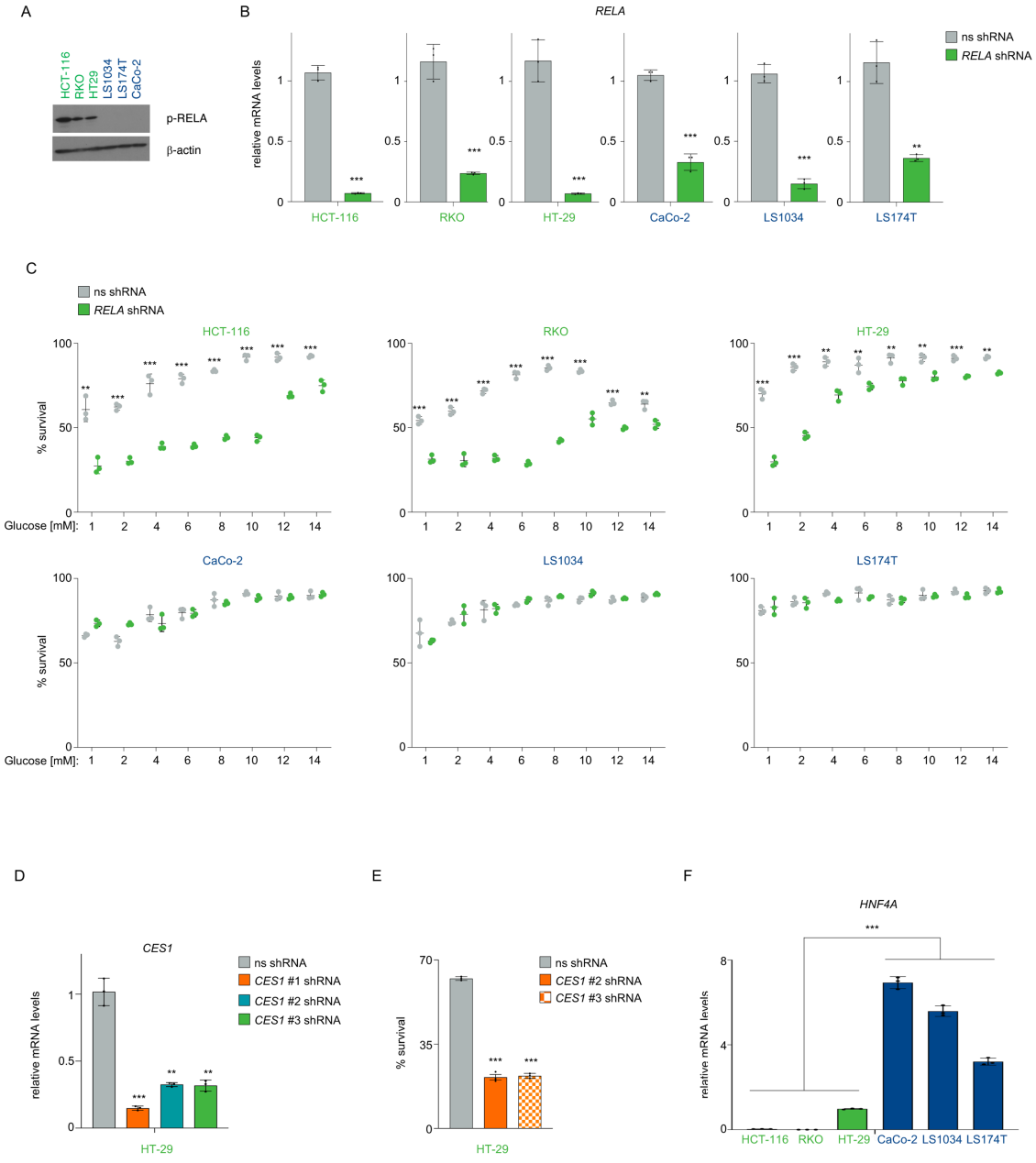
A
HCT-116
RKO
HT29
LS1034
LS174T
CaCo-2
p-RELA
β-actin
B
RELA
relative mRNA levels
ns shRNA
RELA shRNA
HCT-116
RKO
HT-29
CaCo-2
LS1034
LS174T
C
ns shRNA
RELA shRNA
HCT-116
RKO
HT-29
CaCo-2
LS1034
LS174T
% survival
Glucose [mM]: 1 2 4 6 8 10 12 14
D
CES1
relative mRNA levels
ns shRNA
CES1 #1 shRNA
CES1 #2 shRNA
CES1 #3 shRNA
HT-29
E
% survival
ns shRNA
CES1 #2 shRNA
CES1 #3 shRNA
HT-29
F
HNF4A
relative mRNA levels
HCT-116 RKO HT-29 CaCo-2 LS1034 LS174T

FIGURE S6

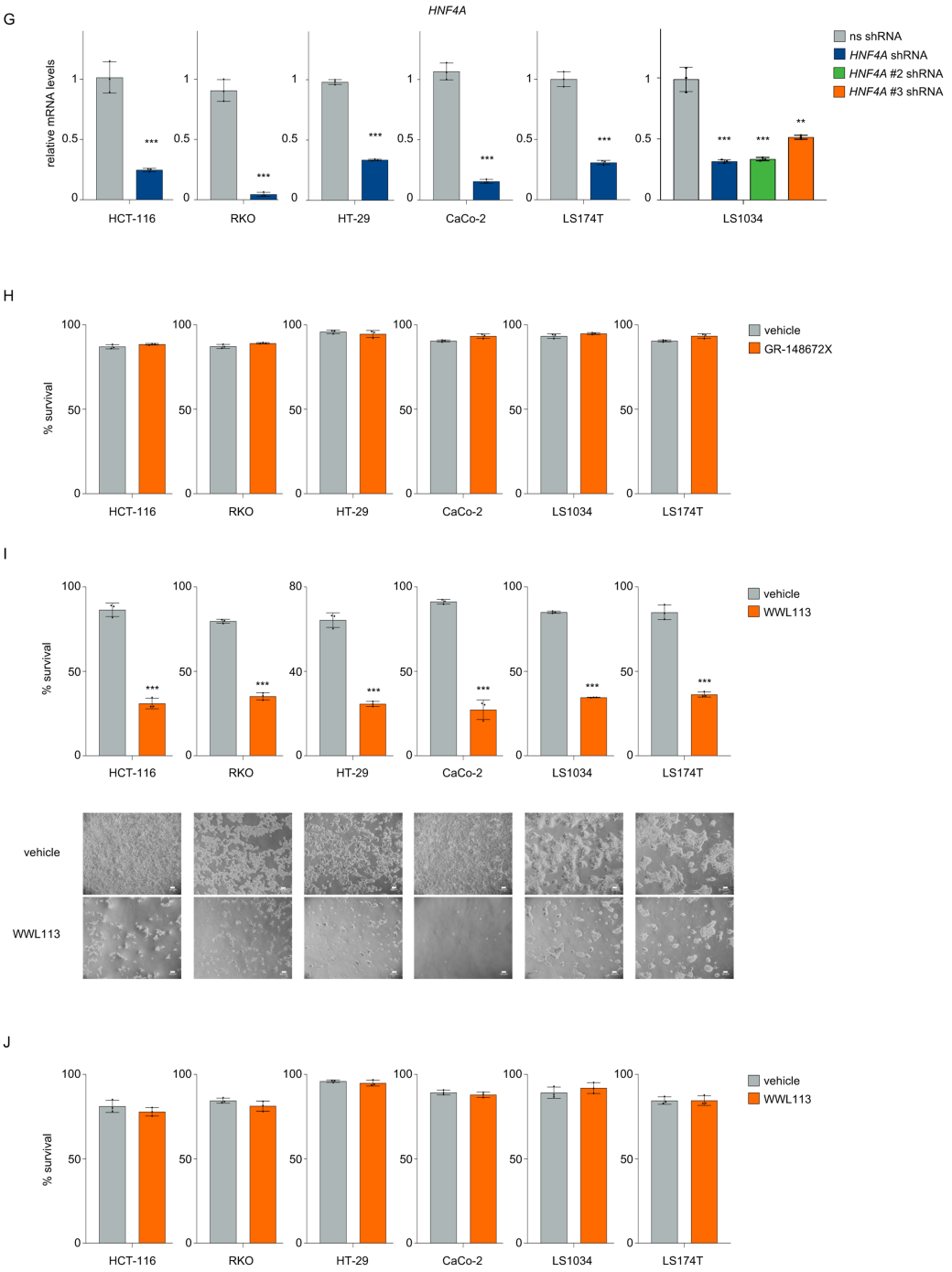

FIGURE S6, related to FIGURE 6. Reciprocal regulation of CES1 by NF-κB and HNF4α in distinct CRCs

A, Western blots showing β-actin and phosphorylated (p) RELA (Ser536) in the indicated human CRC cell lines after a 2-day culture under GL.

B, qRT-PCR showing the mRNA levels of *RELA* in the indicated human CRC cell lines expressing RELA-specific or ns shRNAs, as indicated.

C, Trypan blue exclusion assays showing the percentage of live cells of the human CRC cell lines in (**B**) after a 4-day culture in the presence of the indicated glucose concentrations.

D, qRT-PCR showing the *CES1* mRNA levels in HT29 cells expressing ns or the indicated CES1-specific shRNAs.

E, Trypan blue exclusion assays showing the percentage of live HT-29 cells expressing ns or the indicated additional CES1-specific shRNAs after a 4-day culture under GL.

F, qRT-PCR showing the basal *HNF4A* mRNA expression in the human CRC cell lines from (**B**).

G, qRT-PCR showing the *HNF4A* mRNA levels in the indicated human CRC cell lines expressing HNF4A-specific (HNF4A) or ns shRNAs.

H, Trypan blue exclusion assays showing the percentage of live cells from the indicated human CRC cell lines after a 4-day treatment with GR-148672X or vehicle under normal culture conditions.

I, Trypan blue exclusion assays showing the percentage of live cells from the indicated human CRC cell lines after a 4-day treatment with WWL113 or vehicle under GL (top). Images of representative cells (bottom). Scale bar, 50 μm.

J, Trypan blue exclusion assays showing the percentage of live cells from the indicated human CRC cell lines after a 4-day treatment with WWL113 or vehicle under normal culture conditions.

B-J, Values denote means ± SD (n=3). Statistical significance was calculated using two-tailed Student's t-test. **, p<0.01; ***, p<0.001.

FIGURE S7

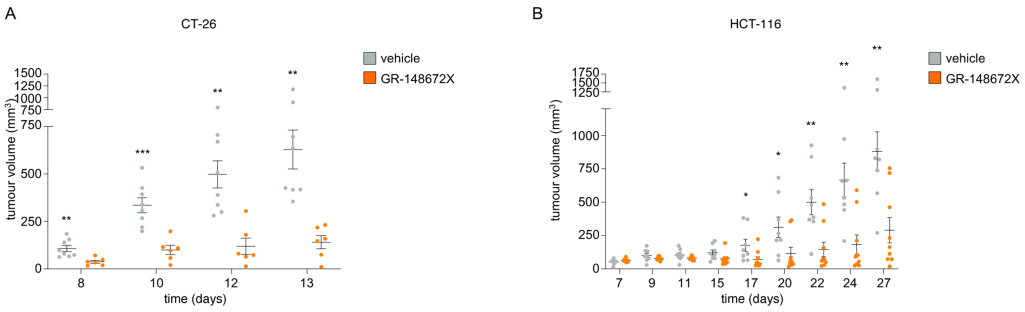

FIGURE S7, related to FIGURE 7. Pharmacologic CES1 inhibition reduces the growth of CRC tumors *in vivo*.

A, Volumes of subcutaneous CT-26 CRC allografts in mice treated as in Figure 7B. All experimental values are plotted.

B, Volumes of subcutaneous HCT-116 CRC xenografts in mice treated as in Figure 7F. All experimental values are plotted.

A-B, Values denote means ± SEM.

A, GR-148672X-treated mice, n=6; vehicle-treated mice, n=8.

B, GR-148672X-treated mice, n=9; vehicle treated mice, n=8.

A-B, Statistical significance was calculated using two-tailed Student's t-test. *, p<0.05; **, p<0.01; ***, p<0.001.

METHODS

Cell culture, viability assays, and lentiviral infection

In-house generated immortalized MEFs and the mouse CT-26 CRC cell line purchased from ATCC were previously described (1). The human CRC cell lines, HCT-116, RKO, HT-29, CaCo-2, LS1034 and LS174T were purchased from ATCC and cultured in accordance with manufacturer's specifications.

Cell line	Medium	Fetal Bovine Serum (FBS)	Additional Components
MEF	high-glucose Dulbecco's modified Eagle's #GIBCO 41965	10%	antibiotics (150U/mL penicillin, 200 U/mL streptomycin), 2mM Glutamine (Gibco)
CT-26, LS1034	ATCC-formulated RPMI-1640 Medium, #ATCC 30-2001.	10%	As above
HCT-116, RKO, HT-29	McCoy's 5a Medium Modified, #ATCC 30-2007	10%	As above
CaCo-2	ATCC-formulated Eagle's Minimum Essential Medium, #ATCC 30-2003	20%	As above
LS174T	ATCC-formulated Eagle's Minimum Essential Medium, #ATCC 30-2003	10%	As above

Cells were cultured in a humidified incubator in 5% CO_2 at 37°C. All cell lines were routinely tested using the Mycoplasma Detection Kit (#ATCC 30-1012K). Cell line authentication (STR) was periodically carried out for all human cell lines. For experiments under glucose limitation (GL), immortalised MEFs were cultured in DMEM without glucose, supplemented with 2% foetal bovine serum (FBS), antibiotics, 2 mM sodium pyruvate, and 6 mM D-glucose. For the GL experiments, CT-26 were cultured as previously described (1). CRC cell lines were cultured in RPMI-1640 medium without glucose, supplemented with 2% FBS, antibiotics, 10 mM HEPES buffer, 1mM sodium pyruvate, and various concentrations of D-glucose as shown in Figure S6C.

Cell viability was assessed by trypan blue exclusion assays conducted as previously reported (1). The production of high-titre lentivirus in HEK293T cells was carried out using Lipofectamine 3000 Transfection Reagent (#L3000015, Thermo

Fisher) in accordance with the manufacturer's specifications. Lentiviral infections were carried out as previously described (1).

The reagents used for cell treatments were the following: oleic acid-BSA solution (200 μM, O3008), etomoxir (10 μM, #E1905), D-(+)-glucose solution (#G8769), ferrostatin-1 (0.5 μM, SML0583), and WWL113 (#SML1179) from Sigma-Aldrich; GR-148672X from Active Biochem; z-VAD-fmk (50 μM, ALX-260-020) from Enzo Life Sciences. The reagents used for pulse-chase labelling experiments were: oleic acid, sodium salt (U-13C18; 200 μM, #CLM-8763) from CK isotopes; fatty acid (FA)-free bovine serum albumin fraction V (#10775835001) from Roche; triacsin C (10 μM, #0007448) from Cayman Chemical; forskolin (10 μM, F3917) and paraoxon E600 (100 μM, #PS610) from Sigma-Aldrich. For treatment of human CRC cell lines, CES1 inhibitors were used as follows: GR-148672X, 10 μM; WWL113, 10 μM (CaCo-2, HT-29), 8 μM (LS1034, LS174T), and 6 μM (HCT-116, RKO). The oleate-BSA conjugation procedure used for the pulse-chase labelling experiments was carried out according to the protocol recommended by Agilent Seahorse.

Lentiviral vectors

The DNA sequences of the shRNAs used for targeting the mouse *RelA* and human *RELA* genes and the non-specific (ns) control DNA sequences in the pLentiLox3.7 lentiviral vector, and the control shc003v sequence in the pLKO.1 lentiviral vector were previously described (1, 2). The DNA sequences of the shRNAs used for targeting the mouse *Ces1d*, human *CES1*, and human *HNF4A* genes in the pLKO.1 lentiviral vector were purchased from Sigma-Aldrich and are listed in the table below:

Gene	Targeting sequence	TRC number
Ces1d	5'-CCGGGCTGCTCTGATTACAACAGATCTCGAGATCTGTTGTAATCAGAG CAGCTTTTTG-3'	TRCN0000031880
Ces1d-2	5'-CCGGGCTGGATCATTCCAACGCTTACTCGAGTAAGCGTTGGAATGATC CAGCTTTTTG-3'	TRCN0000031879
Ces1d-3	5'-CCGGGTGAACACTGTTAAAGGCAAACTCGAGTTTGCCTTTAACAGTGTT CACTTTTTG-3'	TRCN0000031881
CES1	5'-CCGGGAGCTCTTGGAGACGACATTGCTCGAGCAATGTCGTCTCCAAGA GCTCTTTTTG-3'	TRCN0000371770
CES1-2	5'-CCGGATGAGCTCTTCTCCGTCTTTGCTCGAGCAAAGACGGAGAAGAGC TCATTTTTTG-3'	TRCN0000371769
CES1-3	5'-CCGGTGAAACCCAAGACGGTGATAGCTCGAGCTATCACCGTCTTGGGT TTCATTTTTG-3'	TRCN0000371771
HNF4A	5'-CCGGTTGACGCCCTGCTCTGGATAACTCGAGTTATCCAGAGCAGGGCG TCAATTTTTG-3'	TRCN0000364380
HNF4A-2	5'-CCGGTCTTCGGCATGGCCAAGATTGCTCGAGCAATCTTGGCCATGCCG AAGATTTTTG-3'	TRCN0000364314
HNF4A-3	5'-CCGGTCACCTGATGCAGGAACATATCTCGAGATATGTTCCTGCATCAG GTGATTTTTG-3'	TRCN0000376470

The Tween lentiviral vector was previously described (3). The full-length complementary (c)DNA of mouse *Ces1d* was purchased from Eurofins and introduced between the XhoI and EcoRV restriction sites of the Tween lentiviral vector. The mutant, RNAi-resistant *Ces1d*-encoding DNA sequence (*Ces1dM*) used for validation of the Ces1d-specific shRNAs was obtained by site-direct mutagenesis (original DNA sequence: GCT GCT CTG ATT ACA ACA GAT; mutated DNA sequence GC<u>A</u> GC<u>A</u> <u>TT</u>A AT<u>C</u> AC<u>C</u> AC<u>C</u> GA<u>C</u>) and subcloned in the pWPT lentiviral vector (GenScript Biotech, Leiden, Netherlands).

Metabolomic profiling

The metabolomic profiling of MEFs was carried out by Metabolon, Inc. (Morrisville, NC, USA). Cell pellets from MEFs expressing RelA-specific or ns shRNAs and cultured under normal conditions or GL, were prepared in accordance with Metabolon's guidelines, using five biological replicates per condition. Briefly, samples were

prepared using the automated MicroLab STAR® system from Hamilton. Several recovery standards were added for QC purposes prior to the first step in the extraction process. To remove proteins, dissociate small molecules bound to proteins or trapped in the precipitated protein matrix, and to recover chemically diverse metabolites, proteins were precipitated with methanol under vigorous shaking for 2 min (Glen Mills GenoGrinder 2000), followed by centrifugation.

The resulting extract was divided into five fractions: two for analysis by two separate reverse phase (RP)/UPLC-MS/MS methods with positive ion mode electrospray ionization (ESI), one for analysis by RP/UPLC-MS/MS with negative ion mode ESI, one for analysis by HILIC/UPLC-MS/MS with negative ion mode ESI, and one fraction was reserved for backup (4). Samples were placed briefly on a TurboVap® (Zymark) to remove the organic solvent. The sample extracts were stored overnight under nitrogen before preparation for analysis. For QA/QC purposes, several types of controls were analysed in concert with the experimental samples: a pooled matrix sample, generated by taking a small volume of each experimental sample, served as a technical replicate throughout the data set; extracted water samples served as process blanks; and a cocktail of QC standards that were carefully chosen not to interfere with the measurement of endogenous compounds were spiked into every sample analysed, allowed instrument performance monitoring and aided chromatographic alignment. Instrument variability was determined by calculating the median relative standard deviation (RSD) for the standards that were added to each sample prior to injection into the mass spectrometers. Overall process variability was determined by calculating the median RSD for all endogenous metabolites (*i.e.*, non-instrument standards) present in 100% of the pooled matrix samples.

Experimental samples were randomized across the platform run with QC samples spaced evenly among the injections. Ultrahigh Performance Liquid Chromatography-Tandem Mass Spectroscopy (UPLC-MS/MS) was carried out. All

methods utilised a Waters ACQUITY ultra-performance liquid chromatography (UPLC) and a Thermo Scientific Q-Exactive high resolution/accurate mass spectrometer interfaced with a heated electrospray ionization (HESI-II) source and Orbitrap mass analyzer operated at 35,000 mass resolution. The sample extract was dried then reconstituted in solvents compatible to each of the four methods. Each reconstitution solvent contained a series of standards at fixed concentrations to ensure injection and chromatographic consistency. One aliquot was analysed using acidic positive ion conditions, chromatographically optimized for more hydrophilic compounds. In this method, the extract was gradient eluted from a C18 column (Waters UPLC BEH C18-2.1x100 mm, 1.7 µm) using water and methanol, containing 0.05% perfluoropentanoic acid (PFPA) and 0.1% formic acid (FA). Another aliquot was analysed using acidic positive ion conditions; however, it was chromatographically optimized for more hydrophobic compounds. In this method, the extract was gradient eluted from the same aforementioned C18 column using methanol, acetonitrile, water, 0.05% PFPA and 0.01% FA and was operated at an overall higher organic content. A further aliquot was analysed using basic negative ion optimized conditions using a separate dedicated C18 column. The basic extracts were gradient eluted from the column using methanol and water; however, with 6.5 mM ammonium bicarbonate at pH 8. The fourth aliquot was analysed via negative ionization following elution from a HILIC column (Waters UPLC BEH Amide 2.1x150 mm, 1.7 µm) using a gradient consisting of water and acetonitrile with 10 mM ammonium formate, at pH 10.8.

The MS analysis alternated between MS and data-dependent MSn scans using dynamic exclusion. The scan range varied slighted between methods but covered 70-1000 m/z. Raw data files were archived and extracted as described below. Briefly, raw data was extracted, peak-identified and QC processed using Metabolon's hardware and software. Compounds were identified by comparison to library entries of purified standards or recurrent unknown entities (5). Metabolon data analysts used

proprietary visualization and interpretation software to confirm the consistency of peak identification among the various samples. Library matches for each compound were checked for each sample and corrected if necessary. Peaks were quantified using the area-under-the-curve. A data normalisation step was performed to correct variation resulting from instrument inter-day tuning differences. Essentially, each compound was corrected in run-day blocks by registering the medians to equal one (1.00) and normalising each data point proportionately.

The untargeted metabolomic profiling dataset comprises a total of 488 biochemicals. Following normalisation to Bradford protein concentration, log transformation and imputation of missing values, if any, with the minimum observed value for each compound, ANOVA contrasts were used to identify biochemicals that differed between experimental groups. An estimate of the false discovery rate (FDR) was used to take into account multiple comparisons and identify biochemicals present in significantly different abundance (q<0.05). All 488 metabolites were annotated according to “super-pathways” and “sub-pathways” using a Metabolon-based classification. CAMERA (6) was used to test whether a set of metabolites annotated to sub-pathways with at least 5 biochemicals was highly ranked relative to other metabolites in terms of differential abundance. p values were corrected for multiple testing according to the number of sub-pathways tested by using Benjamini and Hochberg false discovery rate method.

Lipid profiling

Lipid profiling in MEFs expressing RelA-specific or ns shRNAs and cultured under normal conditions or GL, was carried out at Metabolon, Inc. using TrueMass® Lipomic Panel. Cell pellets were prepared in accordance with Metabolon’s guidelines, using five biological replicates per condition. Briefly, samples were homogenised in

deionized water. A portion of each homogenate was reserved for Bradford (protein) quantification for normalisation purposes. Lipids were extracted from samples using a modified Bligh-Dyer extraction method in the presence of internal standards. The extracts were concentrated under nitrogen and reconstituted in 0.25 mL of 10 mM ammonium acetate in dichloromethane:methanol (50:50). The extracts were transferred to glass inserts and placed in vials for infusion-MS analysis, performed on a Shimadzu LC with nano PEEK tubing and the SciEx Selexlon-5500 QTRAP. The samples were analysed via both positive and negative mode electrospray. The MS was operated in MRM mode with a total of more than 1,100 MRMs. Individual lipid species were quantified by taking the peak area ratios of target compounds and their assigned internal standards, then multiplying by the concentration of internal standard added to the sample. Lipid class concentrations were calculated from the sum of all molecular species within a class, and FA compositions were determined by calculating the proportion of each class comprised by individual FAs. The Complex Lipid dataset comprises a total of 1,028 biochemicals. Following normalisation to Bradford protein concentration, log transformation and imputation of missing values, if any, with the minimum observed value for each compound, ANOVA contrasts were used to identify biochemicals that differed between experimental groups. An estimate of the FDR was used to take into account multiple comparisons and identify biochemicals present in significantly different abundance (q<0.05). The biochemicals were annotated in classes using a Metabolon-based classification and the hypergeometric test followed by the Benjamini and Hochberg's procedure was used to determine the statistical significance of the enrichment.

For the assessment of TAG turnover, CT-26 cells expressing ns, *RelA* or *Ces1d* shRNAs were pulsed for 4 hr with 200 μM [^{13}C]-oleate:BSA (6:1) to pre-label the endogenous TAG pool. Following the pulse, cells were chased for either 1 or 8 hr, as indicated, in RPMI medium, containing 0.1 mM glucose, 0.5% FA-free BSA and triacsin

C to block FA recycling into the TAG pool, as described previously (7), in the presence of forskolin to stimulate lipolysis. The abundance of the [^{13}C]-labelled TAG pool at the indicated times was measured, and turnover was calculated as the percentage of decrease in the [^{13}C]-labelled TAG pool abundance with respect to the corresponding 0-hr time point. For the assessment of TAG lipogenesis, CT-26 cells were pre-treated for 4 hr with etomoxir and E600, blocking FAO and lipolysis, respectively, and then pulsed for another 4 hr with 200 μM [^{13}C]-oleate:BSA. For lipid profiling, CT-26 cells expressing ns, *RelA* or *Ces1d* shRNAs were cultured in RPMI 1640 medium without glucose, supplemented with 10% FBS, antibiotics, 10 mM HEPES buffer, 1 mM sodium pyruvate, and 14 mM D-glucose. For the lipid profiling of human CRC cell lines, cells expressing ns or *RelA* shRNAs were cultured in RPMI 1640 medium without glucose, supplemented with 2% FBS, antibiotics, 10 mM HEPES buffer, 1 mM sodium pyruvate, and 6 mM D-glucose.

For both lipid profiling and pulse-chase experiments, upon *in vitro* culture, CT-26 cells were washed in cold 1x phospahte buffer saline (PBS) at pH 7.4 (Gibco, 10010023), scraped and then spun down, and cell pellets were flash-frozen in liquid nitrogen. Lipids were extracted from the cell samples by using an appropriate volume (*i.e.*, 1 mL/2.5x10^6 cells) of a methanol:MTBE:chloroform (MMC) mixture (40/30/30, v/v/v)(8), containing 10 μg/100 mL of the antioxidant, 2,6-di-t-butyl-p-hydroxytoluene (BHT). Samples were then vortexed, shaken at room temperature for 30 min (950 rpm), and centrifuged for 10 min at 8,000 rpm. Upon collection into fresh Eppendorf tubes, the supernatants (2 μL) were injected for analysis onto a LC-MS system, consisting of a binary pump, a thermostated autosampler and a column compartment, each from the Dionex UltiMate 3000 series (Thermo Fisher Scientific, Waltham, MA USA), and a Thermo Q-exactive mass spectrometer (Thermo Fisher Scientific, Waltham, MA USA). Liquid chromatography separation was performed at 45°C using a Kinetex F5 reverse-phase column (Phenomenex inc.) at the flow rate of 0.65 ml/min.

The mobile phases consisted of 5 mM ammonium formate and 0.1% formic acid in water (solvent A), and of 5 mM ammonium formate and 0.1% formic acid in isopropanol (solvent B). A gradient elution was used for lipid separation as follows: time 0 min, solvent A 80%, solvent B 20%; time 3 min, solvent A 60%, solvent B 40%; time 16 min, solvent A 40%, solvent B 60%; time 16.5 min, solvent A 30%, solvent B 70%; time 24 min, solvent A 26%, solvent B 74%; time 28 min, solvent A 5%, solvent B 95%; and time 30, stop run. All solvents were purchased from Sigma-Aldrich and Biosolve (Dieuze, FR). In the first step, mass spectrometry analysis was performed in positive/negative ion switching method in Full MS scan mode. The Lipostar software (version 1.0.5, Molecular Discovery Ltd, UK) (9) was then used to perform a pre-identification of potential lipid species on the basis of the m/z and retention time values. The automatic identification of potential lipid species was performed by searching for mass matches within two in-house built libraries of *in silico* fragmented lipids (one library containing approximately 800,000 non-labelled lipids, and another one containing approximately 800,000 [^{13}C]-labelled lipid species potentially generated from the [^{13}C]-oleic acid chain). Inclusion lists of the masses of interest were subsequently generated. In the second step, a reduced number of samples automatically selected by Lipostar software was re-analysed in DDS mode by using the inclusion lists in order to obtain MS/MS data. The MS/MS data were then imported into the data matrix generated by Lipostar to perform the final lipid identification step, based on exact mass, retention time and MS/MS fragmentation. Automatically generated data were visually inspected, and only high-confidence data were ultimately selected for evaluating the behaviour of the identified lipids. For the untargeted metabolic profiling of the human CRC cell lines, two-tailed Student's t-test was used to identify biochemicals that differed between the experimental groups. An estimate of the FDR was used to take into account multiple comparisons and identify biochemicals present in significantly different abundance (q<0.05). Only biochemicals having a value different from zero for the three replicates of the time points investigated were tested.

Hypergeometric test was used to assess whether a lipid class was highly enriched relative to other lipid classes in terms of differential abundance. *p* values were corrected for multiple testing according to the number of performed tested by using Benjamini and Hochberg false discovery rate method.

RNA extraction and quantitative real-time polymerase-chain reaction (qRT-PCR)

Total RNA was extracted using TRIzol RNA isolation reagent (#15596018, Thermo Fisher) and purified by using the Direct-zol RNA MicroPrep or MiniPrep Kit (Zymo Research). The isolated RNA was spectrophotometrically quantified, and equal amounts were used for cDNA synthesis using the GeneAmp RNA PCR Kit (Applied Biosystems). qRT-PCR was carried out on an ABI 7900 real-time PCR machine using the TaqMan® Universal PCR Master Mix (#4304437, Applied Biosystems). Experimental Ct values were normalised to β-actin for cell lines and to UBC for primary CRC samples, and the relative mRNA expression was then calculated using a reference sample. The following predesigned TaqMan® Gene Expression Assays were used:

Gene	Species	Assay ID	Reporter
HNF4A	Human	Hs00230853_m1	FAM
ACTB	Human	Hs99999903_m1	FAM
CES1	Human	Hs00275607_m1	FAM
RELA	Human	Hs00153294_m1	FAM
UBC	Human	Hs00824723_m1	FAM
Ces1d	Mouse	Mm00474816_m1	FAM
RelA	Mouse	Mm00501346_m1	FAM
ACTB	Mouse	Mm01304398_m1	FAM

mRNA sequencing

Illumina RNA sequencing was carried out at Novogene (Beijing, China). RNA degradation and sample contamination were monitored on 1% agarose gels. RNA purity was determined using a NanoPhotometer® spectrophotometer (IMPLEN, CA, USA). RNA concentration was assessed using the Qubit® RNA Assay Kit and a Qubit® 2.0 Flurometer (Life Technologies, CA, USA). RNA integrity was verified using the RNA Nano 6000 Assay Kit and a Bioanalyzer 2100 system (Agilent Technologies, CA, USA). For library preparation, a total amount of 3 μg of RNA per sample were used as input material. Sequencing libraries were generated by using the NEBNext® Ultra™ RNA Library Prep Kit from Illumina® (NEB, USA) according to manufacturer's recommendations, and index codes were added to attribute the sequences in each sample. Briefly, mRNA was purified from total RNA using poly-T oligo-attached magnetic beads. mRNA fragmentation was carried out using divalent cations under conditions of elevated temperature in 5x NEBNext First Strand Synthesis Reaction Buffer. The first strand cDNA was synthesized using random hexamer primers and M-MuLV Reverse Transcriptase (RNase H^-). The second strand cDNA synthesis was subsequently carried out using DNA Polymerase I and RNase H. The remaining overhangs were converted into blunt ends by using exonuclease/polymerase activities. After adenylation of the 3' ends of DNA fragments, NEBNext Adaptor with hairpin loop structures were ligated to prepare for hybridization. In order to preferentially select cDNA fragments of 150-200 bp in length, library fragments were purified using an AMPure XP system (Beckman Coulter, Beverly, USA). 3 μL of USER Enzyme (NEB, USA) were then incubated with the size-selected, adaptor-ligated cDNA for 15 min at 37°C followed by 5 min at 95°C prior to the qPCR reaction. qPCR was performed using Phusion High-Fidelity DNA polymerase, Universal PCR primers and Index (X) Primer. qPCR products were finally purified (AMPure XP system), and library quality was assessed by using an Agilent Bioanalyzer 2100 system. The clustering of index-coded samples was performed on a cBot Cluster Generation System, using the HiSeq PE Cluster Kit cBot-HS (Illumina), according to the manufacturer's instructions.

After cluster generation, the library preparations were sequenced on an Illumina Hiseq platform, and 150 bp paired-end reads were generated. Raw reads containing adapters and poly-N sequences were filtered out, and only high-quality reads (>Q20) were considered for further analysis. Paired-end reads were then aligned to the reference genome, GRCm38, using TopHat v2.0.12 with mismatch parameter sets at two, and the other parameters set to default. HTSeq v0.6.1 was used to count the number of reads mapped to each gene and calculate the Fragments Per Kilobase of transcript per Million (FPKM) using Novogene in-house scripts. The differential expression analysis of *RelA*-deficient compared to control MEFs, using five biological replicates per condition, was conducted using the DESeq R package (1.18.0). The resulting *p* values were adjusted using the Benjamini and Hochberg's approach for controlling the FDR. Genes with an adjusted *p* value <0.05 were considered to be differentially expressed. For each time points, genes were ranked according to fold change, and the intersection among the top 20 most downregulated genes was used to identify the subset of genes having a human orthologue whose fold change was most markedly downregulated in RelA-deficient relative to control MEFs across all time points investigated. For Volcano plots, the lists of the metabolic genes present in the Reactome database (n=1,792) were downloaded using Ensembl (version 67, 2018). For each time point, only genes with at least 50 counts in either RelA deficient or control MEFs were considered for further analysis.

Chromatin immunoprecipitation

Chromatin immunoprecipitation in CT-26 cells expressing *RelA*-specific or ns shRNAs was carried out as previously described (1, 10). Briefly, upon culture under normal conditions or GL, CT-26 cells were treated with 1% formaldehyde for 10 min at room temperature in order to crosslink the protein-DNA complexes. After quenching the

reactions using 125 mM glycine, chromatin extracts were sonicated with a Bioruptor sonicator (Diagenode), and protein-DNA complexes were immunoprecipitated using anti-RelA or control IgG antibodies. Quantitative PCR (qPCR) assays were then carried out using the anti-RelA and IgG precipitates as templates and the indicated primers encompassing the NF-κB-binding DNA (κB) elements identified in the promoter and intronic regions of the *Ces1d* gene or control genomic regions (controls 1-4), in order to assess the NF-κB/RelA DNA-binding specificity. RelA-specific DNA binding was calculated relative to the background signal yielded by the control IgG antibody and expressed as fold change. The qPCR primers used are listed in the table below:

Name	Forward Primer	Reverse Primer	Position
Ces1d κB1	5'-TGTGTTGTCTGCTTTACCACA-3'	5'-GGGTGCCCTATGACTGTCA-3'	*Ces1d* intron 1
Ces1d κB2	5'-ATGTTCAGGAAGGGCAAGGT-3'	5'-TGCTTATTCCAAAGGGCTCA-3'	*Ces1d* promoter
Ces1d κB3	5'-AAACTGCACACCCTTCTCCC-3'	5'-TGCTGCTTATCTGATACACACA-3'	*Ces1d* promoter
Ces1d κB4	5'-AGAAGTGGCTTTCTGGACTGA-3'	5'-CTCCCACCACACAATTCTGC-3'	*Ces1d* intron 2
Ces1d κB5	5'-GTCCTCACATCCCAGCTGAG-3'	5'-CCTCAATTCAGTGCACCCTG-3'	*Ces1d* promoter
Ces1d κB6	5'-ACAACGTGCTTAAATCAGACAAT-3'	5'-GGCCTCCTGACTAACCTCATT-3'	*Ces1d* intron 1
Ces1d κB7	5'-TGACATAGAGGCTGGATTCCA-3'	5'-CTCCCCTGGTGTCCTCTTTG-3'	*Ces1d* intron 1
Ces1d κB8	5'-GGGTGCATCAAAGTCCGAAG-3'	5'-TGATCCTTCTTCAGCTCTCCT-3'	*Ces1d* intron 1
Ces1d κB9	5'-AGTTTGCAAAGCCTGGGT-3'	5'-ACCTTTTGCCTACCTTTTAACCT-3'	*Ces1d* intron 1
Ces1d κB10	5'-CCCATCAAGTCCAGATAGCCTA-3'	5'-GCAGTAGTAAGGACACCACCA-3'	*Ces1d* intron 2
Control 1	5'-CATGGTGCAGCAAACCAACA-3'	5'-TTCCTTTTCCTGCCACGCTGT-3'	SOX4
Control 2	5'-CTAATAGTCCCATGCTCTCC-3'	5'-TCCTTCCTTTGGTGGCTTC-3'	Ig-κLC promoter
Control 3	5'-TGTGTTTGCTAAGGCTTCAGTG-3'	5'-TCATGGTTGGTCAGCTATCCC-3'	*Ces1d* exon
Control 4	CAATGACTACAGCCTCCATTGATGT-3'	5'-AGAAAAACATTCAAGGCCATCCAA-3'	*Ces1d* exon

Luciferase assays

Ten DNA regions from the murine *Ces1d* locus on chromosome 8 that contained the NF-κB-binding sites identified by ChIP were subcloned into the NanoLuc luciferase reporter vector, pNL3.2[NlucP/minP] (Promega) (GenScript Biotech, Leiden, Netherlands) as follows:

Name	*Start [negative strand; 5'-3']*	*End [negative strand; 5'-3']*	*Length (bp)*
Ces1d κB1	*93197427*	*93197523*	*96*
Ces1d κB2	*93199824*	*93199920*	*96*
Ces1d κB3	*93195010*	*93197523*	*120*
Ces1d κB4	*93201537*	*93201633*	*96*
Ces1d κB5	*93194204*	*93194400*	*96*
Ces1d κB6	*93198483*	*93198579*	*96*
Ces1d κB7	*93199378*	*93199511*	*133*
Ces1d κB8	*93198081*	*92198177*	*96*
Ces1d κB9	*93198285*	*93198381*	*96*
Ces1d κB10	*93200988*	*93201084*	*96*
Negative Control	*93200988*	*93201084*	*96*

70 ng of each plasmid or the negative control vector and 30 ng of the firefly luciferase reporter vector, pGL4.54[luc2/TK], were co-transfected in HEK-293T cells expressing *RelA*-specific or ns shRNAs and seeded in a white 96 well plate using Lipofectamine 3000. The pNL3.2.NF-κB-RE[NlucP/NF-κB-RE/Hygro] Vector containing three copies of an NF-κB-response element (NF-κB-RE) was used as positive control. The day after transfection, cells were cultured under GL conditions for 24 hr, and luciferase activity was assessed using the Nano-Glo® Dual-Luciferase® Reporter Assay System and normalized to firefly luciferase activity. Site-direct mutagenesis (GenScript Biotech, Leiden, Netherlands) was used to mutate each of the NF-κB-binding elements producing significant luciferase activity in response to GL, as shown in the table below:

	Original sequence	*After mutagenesis*
Ces1d κB1	gaaggacccc	cttcgaagag
Ces1d κB2	gggtcttccc ggactcctcc	cttcctagag cttctcagag
Ces1d κB4	tgaaagcccc ggaattctcc	cttcagagag cttcttagag
Ces1d κB7	Ggagttttca ggaaatttcc gggatgttct	cttcttagag cttcatagag cttctgagag

Ces1d κB8	gggataccca	cttctaagag
Ces1d κB10	gaagaattcc	cttcaaagag

Western blots, serine esterase activity-based assays, and antibodies

Western blots were performed as previously described (1, 11). Briefly, proteins were extracted using the following lysis buffer: 50 mM Tris-HCl (pH 7.4), 150 mM NaCl, 1% Triton X-100, and 1 mM EDTA supplemented with Complete Mini Protease Inhibitor Cocktail (11 836 153 001, Roche), 1 mM sodium orthovanadate (S6508, Sigma-Aldrich), and 50 mM sodium fluoride (S7920, Sigma-Aldrich). The antibodies used were as follows: anti-RelA (1:3,000; ADI-KAS-TF110-F, Enzo Life Science); anti-CES1 (1:3,000; NBP1-40430, Novus Biological; or 0.2 μg/mL; AF4920, R&D Systems); anti-p-Hsl (ser660) (1:500; PA5-64494, Thermo Fisher Scientific); anti-Gpx4 (1:1,000; ab125066, Abcam); anti-p-NF-κB/RELA (Ser536) (1:1,000; #3033, Cell Signaling Technology); anti-β-Actin (C4; 1:1,000; sc-47778, Santa Cruz Biotechnology). The anti-RelA NF-κB/p65 antibody (C-20; 1:1,000; sc-372) and rabbit control IgG (1:1,000; sc-109X) used for chromatin immunoprecipitation were from Santa Cruz Biotechnology. For serine esterase activity-based assays, proteins were extracted using the abovementioned lysis buffer supplemented with the same cocktail of protease and phosphatase inhibitors. Cell lysates were incubated with the activity-based ActivX™ Desthiobiotin-FP Serine Hydrolase Probe (#88317, Thermo Fisher Scientific) for selective covalent labelling of active serine hydrolases. FP probe-bound proteins in the cell lysates were enriched by using Pierce High Capacity Streptavidin Agarose Resin (#10302384, Thermo Fisher Scientific), followed by SDS-PAGE and subsequent western-blot detection with an anti-Ces1d antibody. β-actin was measured as a

loading control in the total cell lysates (input) used for the activity-based protein profile (ABPP) assays.

Flow cytometry

Flow cytometry analysis was conducted with CT-26 cells expressing *Ces1d*-specific or ns shRNAs after culture under basal conditions or for the indicated times under GL. For the detection of ROS formation, CT-26 cells were loaded with 500 nM of CellROX™ Green dye (#C10492, Thermo Fisher Scientific) for 1 hr at 37°C and then processed according to the manufacturer's specification. For the detection of lipid peroxidation, CT-26 cells were loaded with 10 μM of C11-BODIPY 581/591 C11 (D3861, Thermo Fisher Scientific) for 3 hr at 37°C and then processed according to the manufacturer's specification. For the assessment of mitochondrial membrane potential (ΔΨm), CT-26 cells were loaded with 10 μM of JC-1 dye (T3168, Thermo Fisher Scientific) for 20 min at 37°C and then processed according to the manufacturer's specification. The intracellular levels of reduced glutathione (GSH) in CT-26 cells were measured using the intracellular GSH kit (ab112132) from Abcam, according to the manufacturer's instructions. The staining of CT-26 cells with Annexin V-FITC and 7-AAD (#640922, Biolegend) was performed according to the manufacturer's instructions. Nucleosomal DNA fragmentation in CT-26 cells was assessed using propidium iodide (PI) (#550825, BD Biosciences) nuclear staining assays conducted as previously described (2). Data were acquired using a LSR II flow cytometer (BD, Biosciences) and analyzed using FlowJo software.

Spectrophotometric assays

Analyses were conducted using CT-26 cells expressing *Ces1d*-specific or ns shRNAs and cultured under basal conditions or for the indicated times under GL. The DCFDA Cellular ROS Detection Assay Kit (#ab113851, Abcam) was used for the measurement of cellular ROS levels according to the manufacturer's specifications. The GSH-Glo™ Glutathione Assay (#V6911, Promega) was used for the measurement of GSH levels according to the manufacturer's specifications. The Lipid Peroxidation (4-HNE) Assay Kit (#ab238538, Abcam) was used for the measurement of 4-HNE-protein adduct levels according to the manufacturer's specifications. The Caspase-Glo® 3/7 Assay System (#G8090, Promega) was used for the measurement of caspase 3/7 activity according to the manufacturer's specifications. The Cell Meter™ Live Cell TUNEL Apoptosis Assay Kit – Red Fluorescence (#22844, Stratech Scientific Ltd) was used for the measurement of nucleosomal DNA fragmentation according to the manufacturer's specifications. In all cases, values were normalized on a per-cell basis.

Oxygen consumption rate (OCR), spare respiratory capacity (SRC), and ATP production rate

For bioenergetic profiling, CT-26 cells expressing *RelA*-specific, *Ces1d*-specific or ns shRNAs were seeded onto wells of Seahorse 96-well plates coated with 0.1% Collagen Type I (#C3867, Sigma Aldrich). Mitostress tests were conducted using a XF-96 Extracellular Flux Analyzer (Agilent Seahorse), and oxygen consumption rates (OCR) was measured in XF Assay Medium (#102365, Agilent Seahorse) containing 1 mM pyruvate, 2 mM glutamine, and 10 mM glucose, following injection of 10 μM etomoxir (#E1905, Sigma Aldrich), 2.8 μM oligomycin A (#75351, Sigma Aldrich), 60 μM 2,4-Dinitrophenol (2,4-DNP; #D198501, Sigma Aldrich), 0.6 μM rotenone (#R8875, Sigma Aldrich), and 0.6 μM antimycin A (#A8674, Sigma Aldrich), as indicated. Cell pre-treatment with oleic acid-BSA solution or BSA was conducted where indicated. All

values were normalized on a per-cell basis. Non-mitochondrial respiration was defined as the minimum oxygen consumption rate recorded after treatment with rotenone/antimycin A. Spare respiratory capacity (SRC) was calculated in accordance to the manufacturer's specifications as the difference between maximal respiration (*i.e.*, the maximum rate measurement recorded after 2,4-DNP injection after subtracting the non-mitochondrial respiration rate) and basal respiration (*i.e.*, the last measurement recorded prior to oligomycin A injection after subtracting the non-mitochondrial respiration rate). ATP production rates were measured using the XF Real-Time ATP Rate Assay Kit (103592-100, Agilent Seahorse) detecting mitochondrial OCR and glycolytic Extra-Cellular Acidification Rates (ECAR), which were then transformed into mitochondrial (mito-ATP) and glycolytic (glyco-ATP) ATP production rates, using validated algorithms provided in the Seahorse Agilent software.

CRC patients and human CRC datasets

Patients were recruited from the Imperial College Healthcare NHS Trust and The Royal Marsden NHS Trust. Patients' electronic records were screened for suitability prior to attendance at the hospital. Patients were recruited prior to undergoing colorectal surgery. Clinical data were collected prospectively, including patient demographics, presenting symptoms, medical and drug history, dietary information, smoking and alcohol intake, and neo-adjuvant oncological treatment. Immediately following surgical resection, fresh colonic specimens were taken to the histology department and opened by a histopathologist. Sterile water was washed gently over the mucosal surface to remove adherent faecal matter. Tissue samples were cut from the tumour and normal mucosa at 10 cm from the tumour site using separate sterile blades by a histopathologist independent from the study team. Each tissue sample was then divided into ~50 mg aliquots using the same sterile blade. An aliquot was

homogenized in gentleMACS M Tubes (#130-093-236, Miltenyi Biotec) using a gentleMACS Dissociator (Miltenyi Biotec), and RNA was then extracted to evaluate *CES1* expression. Further tissue aliquots were stored at -80°C for use in the UPLC-MS profiling.

Data from CRC patients with primary tumours were considered for further analysis. Organic phase tissue extractions were performed. The protocol used was adapted from previously published methods (12, 13). Briefly, a solution of methyltertbutylether/methonol (3:1) was pre-chilled on ice. The pre-chilled methanol/water solution was then added to the tissue pellet (including zirconium beads), in proportions of 100 µL of solvent per 10 mg of tissue. The samples underwent serial bead-beating steps at 6,500 Hz for 40 sec, followed by a 15 sec interval, and again at 6,500 Hz for a further 40 sec. The samples were returned to dry ice for five min before repeating the bead-beating cycles. Following bead-beating, the samples were centrifuged at 13,000 x g for 20 min at 4°C to obtain supernatants. A 100 µL aliquot of each supernatant was then transferred onto glass vials, and these were dried under nitrogen gas flow. The dried samples were stored at -80°C pending reconstitution. Prior to the RP-UPLC-MS run (lipid profiling), the dried organic extracts were thawed at room temperature and reconstituted in 500 µL of a water/ACN/isopropanol (1:1:3) solvent mixture. The samples were briefly vortexed and stored for 72 hr at 4°C. Following a further brief vortex, gentle centrifugation was performed at 200 x g for 2 min at 4°C. 450 µL of supernatant were obtained from each sample and transferred onto 96-well plates. 50 µL were taken from each sample for QC. Analytical plates were dried down under nitrogen gas flow, due to rapid evaporation of reconstitution medium during formatting. For analysis, plates were reconstituted with 450 µL of a water/ACN/isopropanol (1:1:3) solvent mixture, heat-sealed, shaken and then centrifuged. 100 µL were aliquoted from each well into 350 µL plates for the lipid positive and lipid negative analyses, as well as a backup plate.

75 µL of QC was added to columns 11 and 12 in order to replace MR and SR. Plates were immediately heat-sealed. Lipid positive plates were run immediately after preparation. Lipid negative and backup plates were stored at -40°C, pending further analysis. Samples were prepared in a 96-well plate format. To ensure a standard period for analysis, cycles of 15 min were used, allowing the analysis of a single plate within 24 hr. Sample handling was performed with a Waters 2777C sample manager (Waters Corp., Milford, MA, USA). Chromatography was conducted on an ACQUITY UPLC (Waters Corp., Milford, MA, USA), and mass spectrometry used a Xevo G2-S oaTOF MS (Waters Corp., Manchester, UK), which were coupled via a Zspray electrospray ionisation (ESI) source. Untargeted peak detection, alignment, grouping, integration and deisotoping were performed on each full data set using Progenesis QU 2.1 software (Waters Corp., Manchester, UK). Pearson correlation coefficients between the QC sample dilution factor and the extracted signal intensity for the pre- and post-sample analysis dilution series were calculated. The rationale for this approach was to assess the response of each feature to sample dilution, because features that were not correlated to the gradient of concentration in the dilution series were unreliable and as such excluded from the data set (14). A threshold of 0.7 was set. Accurate m/z measurements and retention times of detected chromatographic peaks were matched to the compounds found in the Metlin (13), HMDB (15) and Lipidmaps (16) databases. In addition, confirmation of identities was performed using Tandem MS (MS/MS) on selected ions at their respective retention times. The target ions were fragmented with energies of 5-20 eV to yield daughter ions. The resultant metabolite-specific spectra permitted a more accurate annotation of the peaks and helped to distinguish metabolites with similar m/z ratios. For TAG content and survival analyses, patients were stratified into two groups on the basis of the *CES1* mRNA expression using quartiles as thresholds. The body mass index (BMI) cut-off of 25 kg/m^2, which defines overweight patients according to the current WHO classification (17), was used for the analyses.

Data from the analysis of The Cancer Genome Atlas (TCGA) CRC (COADRED) program and the French National Cartes d'identité des Tumeurs (FNCIT) program (18) were classified according to the CMS subtypes described by the Colorectal Cancer Subtyping Consortium (CRCSC) (19) and downloaded using the Synapse browser (ID: syn2623706). Only patients with a defined CMS subtype were considered for further analysis. For the TCGA dataset, only patients with gene expression profiling conducted by using an Illumina HiSeq 2000 RNA sequencer were considered for analysis (ID: syn2326100). For hierarchical clustering, the Z score-normalised gene expression values from 296 CRCs (comprising 42 CMS1, 119 CMS2, 45 CMS3, and 90 CMS4 tumours) were filtered in order to include 1,795 consistent, but variably expressed metabolic genes (MAD>10%, 0.226) out of a total of 20,500 genes present in the dataset. The list of 1,795 metabolic genes was derived from the Reactome database (version 67) and downloaded using PathwayBrowser (version 3.6). Hierarchical clustering of metabolic genes was performed using Pearson's correlation matrix of the genes and CRC patients within individual CMS subtypes, using Ward's linkage criterion and 1-r as the distance function, where r is the pairwise Pearson's correlation coefficient. The reported heatmap was designed by using the ComplexHeatmap R package. The obesity (20-22), inflammatory (GO:0002673; downloaded from the Molecular Signatures Database; MsigDB, version 6.2) and NF-κB-activation (23) gene signatures were scaled according to the Z-scores, and the average values were used as the scores for the respective gene signatures.

Intracellular human TAG lipases were identified as the enzymes exhibiting triacylglycerol (TAG) lipase activity in the Gene Ontology database (GO:0004806). Pearson's correlation analyses between *CES1* and *HNF4A* mRNA expression, and between *CES1* mRNA expression and the NF-κB target-gene signature were performed for patients from the TCGA dataset considering the Z-scores for gene expression and the average of the Z-score for the gene signature. For correlations,

CES1 expression was plotted against *HNF4A* expression in the CMS1-3 subtypes (n=206), excluding patients with the CMS4 subtype, exhibiting elevated NF-κB target-gene signature, and reciprocally, against the NF-κB target-gene signature in the CMS1 and CMS3-4 subtypes (n=160), excluding patients with the CMS2 subtype, exhibiting an enrichment in *HNF4A* gene amplifications. The data used for DNA Copy-Number Variation (CNV) analysis were derived from The Cancer Genome Atlas Network (24) and downloaded using the UCSC Xena Browser (GISTIC 2 Thresholded values). Briefly, the CNV profile was determined by using the whole-genome microarray analysis conducted by the TCGA COADRED program. The GISTIC 2 method (25) was subsequently applied by using the TCGA FIREHOSE pipeline, in order to produce gene-level CNV estimates and transform them into -2, -1, 0, 1 and 2 thresholds, representing homozygous gene deletion, single copy gene deletion, diploid normal copy number, low-level gene copy number amplification and high-level gene copy number amplification, respectively. Genes were then mapped onto the human genome coordinates, using UCSC Xena HUGO probeMap. Expression values derived from the same sample, but from different vials/portions/analytes/aliquots of that sample were averaged. Disease Specific Survival (DSS) and Progression Free Interval (PFI) data were derived from the TCGA Pan-Cancer Atlas publication by Liu and colleagues (26) and downloaded from the Genomic Data Common repository (https://gdc.cancer.gov/node/905/).

Animal studies

Mice were housed in the animal facilities at Hammersmith Campus, Imperial College London. For allograft experiments, 6-to-8-week old BALB/c nude male mice (CAnN.Cg-*Foxn1*^{nu}/Crl, Charles River) were subcutaneously injected with 1x10^5 CT-26 mouse CRC cells resuspended in 200 µL of sterile PBS (1x) and Matrigel (1:1; BD

Biosciences) using a 1-mL Luer-Lok™ Tip syringe (BD Biosciences) with a 25-gauge needle, as previously described (11). For these experiments, CT-26 cells were harvested from exponentially growing cultures, washed once with serum-free medium and re-suspended in 1x PBS immediately before injection. For *in vivo* administration, GR-148672X was dissolved in DMSO at the final concentration of 100 mM and then diluted in 2% Tween 80/saline solution to a stock concentration of 5 mg/mL. Three days after the injection of the cells, mice were randomized into treatment groups and then treated intraperitoneally with GR-148672X (50 mg/kg of body weight; n=6) or vehicle (n=8), twice a day between day 3 and day 8, and subsequently, once a day between day 9 and day 12, as indicated. Tumour volumes (mm^3) were measured at the indicated times and estimated from calliper measurements using the following formula: volume=$A \times B^2/2$ (with A being the larger diameter, and B the smaller diameter of the tumour). At the experimental endpoint on day 13, mice were sacrificed, and tumours were weighted and photographed.

For xenograft experiments, 6-to-8-week old athymic nude female mice (Crl:NU(NCr)-*Foxn1*^{nu}, Charles River) were subcutaneously injected with $5x10^6$ HCT-116 human CRC cells resuspended in 200 µL of sterile PBS (1x) and Matrigel (1:1), as described above. For these experiments, HCT-116 cells were harvested from exponentially growing cultures, washed once with serum-free medium and re-suspended in 1x PBS immediately before injection. Eight days after the injection of the cells, mice were randomized into treatment groups and then treated intraperitoneally with GR-148672X (50 mg/kg of body weight; n=9) or vehicle (n=8), twice a day between day 8 and day 13, and subsequently, once a day between day 14 and day 26, as indicated. Tumour volumes were measured at the indicated times as described above. At the experimental endpoint on day 27, mice were sacrificed, and tumours were weighted and photographed.

Statistics

For the analysis of biological data (excluding data from the metabolomic, transcriptomic and genomic analyses), the statistical significance for two-sample comparisons was calculated using two-tailed Student's t-test or two-tailed Mann-Whitney U-test, depending on the distribution of the data, as indicated. The statistical significance for multiple-sample comparisons was calculated using one-way ANOVA or the Kruskal-Wallis test, as indicated. The normality of the data distributions and homogeneity of variances were evaluated for appropriateness prior to conducting the statistical tests and were assessed by using Shapiro-Wilk's and Bartlett's test, respectively. Where more than one statistical test was performed, *p* values were corrected for multiple testing by using the Benjamini-Hochberg method. Differences were considered to be statistically significant if the *p* value, after correction in the case of multiple tests, was lower than 0.05. Exact *p* values or adjusted *p* values and group size (n) are reported in each Figure Legend. For the analysis of DSS and PFI, patients at stages 0-3 of the disease, as defined by the American Joint Committee on Cancer (AJCC), and with available survival data were considered. For the analysis of data from the TCGA dataset, patients with less than 5 months of follow-up were excluded from the analysis of DSS. CRC patients were stratified into two groups on the basis of the *CES1* mRNA expression, using either the first or second quartile as threshold (*i.e.*, 25% and 50% of the dataset, respectively). The first quartile was identified as a biologically appropriate threshold for the analysis of the correlations between *CES1* mRNA expression and clinical outcome. The median was used as stratification threshold for the in-house CRC patient dataset [n=59], given the dataset size. Survival curves were estimated using the Kaplan-Meier method, and statistical differences were tested using the log-rank test. *p* values <0.05 were considered to be statistically significant. All analyses were performed using RStudio software (R version 3.4.4).

Study approval

A prospective, observational study of patients at serial stages along the CRC disease pathway was conducted between January 2015 and January 2017. Ethical approval for this study was provided by the Research Ethics Committee and Health Research Authority (REC reference: 14/EE/0024). Informed written consent was obtained from all the subjects involved in the studies. Mouse experiments were conducted under the authority of Home Office PPL P57F16A53. The PPL was approved by the Imperial College Ethical Review Process (ERP) and the Home Office.

SUPPLEMENTARY REFERENCES

1. Mauro C, Leow SC, Anso E, Rocha S, Thotakura AK, Tornatore L, et al. NF-kappaB controls energy homeostasis and metabolic adaptation by upregulating mitochondrial respiration. *Nat Cell Biol.* 2011;13(10):1272-9.

2. Tornatore L, Sandomenico A, Raimondo D, Low C, Rocci A, Tralau-Stewart C, et al. Cancer-selective targeting of the NF-kappaB survival pathway with GADD45beta/MKK7 inhibitors. *Cancer Cell.* 2014;26(4):495-508.

3. Ricci-Vitiani L, Pedini F, Mollinari C, Condorelli G, Bonci D, Bez A, et al. Absence of caspase 8 and high expression of PED protect primitive neural cells from cell death. *J Exp Med.* 2004;200(10):1257-66.

4. Evans AM BB, Liu Q, Mitchell MW, Robinson RJ, Dai H, Stewart SJ, DeHaven CD and Miller LAD. High Resolution Mass Spectrometry Improves Data Quantity and Quality as Compared to Unit Mass Resolution Mass Spectrometry in High-Throughput Profiling *Metabolomics.* 2014;4(2):e1000132.

5. DeHaven CD, Evans AM, Dai HP, and Lawton KA. Organization of GC/MS and LC/MS metabolomics data into chemical libraries. *J Cheminformatics.* 2010;2.

6. Wu D, and Smyth GK. Camera: a competitive gene set test accounting for inter-gene correlation. *Nucleic Acids Res.* 2012;40(17).

7. Laurens C, Bourlier V, Mairal A, Louche K, Badin PM, Mouisel E, et al. Perilipin 5 fine-tunes lipid oxidation to metabolic demand and protects against lipotoxicity in skeletal muscle. *Sci Rep-Uk.* 2016;6.

8. Pellegrino RM, Di Veroli A, Valeri A, Goracci L, and Cruciani G. LC/MS lipid profiling from human serum: a new method for global lipid extraction. *Anal Bioanal Chem.* 2014;406(30):7937-48.

9. Goracci L, Tortorella S, Tiberi P, Pellegrino RM, Di Veroli A, Valeri A, et al. Lipostar, a Comprehensive Platform-Neutral Cheminformatics Tool for Lipidomics. *Anal Chem.* 2017;89(11):6257-64.

10. Fullwood MJ, Liu MH, Pan YF, Liu J, Xu H, Bin Mohamed Y, et al. An oestrogen-receptor-alpha-bound human chromatin interactome. *Nature.* 2009;462(7269):58-64.

11. Verzella D, Bennett J, Fischietti M, Thotakura AK, Recordati C, Pasqualini F, et al. GADD45beta Loss Ablates Innate Immunosuppression in Cancer. *Cancer Res.* 2018;78(5):1275-92.

12. Anwar MA, Vorkas PA, Li JV, Shalhoub J, Want EJ, Davies AH, et al. Optimization of metabolite extraction of human vein tissue for ultra performance liquid chromatography-mass spectrometry and nuclear magnetic resonance-based untargeted metabolic profiling. *Analyst.* 2015;140(22):7586-97.

13. Vorkas PA, Isaac G, Anwar MA, Davies AH, Want EJ, Nicholson JK, et al. Untargeted UPLC-MS Profiling Pipeline to Expand Tissue Metabolome Coverage: Application to Cardiovascular Disease. *Analytical Chemistry.* 2015;87(8):4184-93.

14. Croixmarie V, Umbdenstock T, Cloarec O, Moreau A, Pascussi JM, Boursier-Neyret C, et al. Integrated Comparison of Drug-Related and Drug-Induced Ultra Performance Liquid Chromatography/Mass Spectrometry Metabonomic Profiles Using Human Hepatocyte Cultures. *Analytical Chemistry.* 2009;81(15):6061-9.

15. Wishart DS, Knox C, Guo AC, Eisner R, Young N, Gautam B, et al. HMDB: a knowledgebase for the human metabolome. *Nucleic Acids Res.* 2009;37:D603-D10.

16. Fahy E, Sud M, Cotter D, and Subramaniam S. LIPID MAPS online tools for lipid research. *Nucleic Acids Res.* 2007;35:W606-W12.

17. http://www.euro.who.int/en/health-topics/disease-prevention/nutrition/a-healthy-lifestyle/body-mass-index-bmi.

18. Marisa L, de Reyniès A, Duval A, Selves J, Gaub MP, Vescovo L, et al. Gene expression classification of colon cancer into molecular subtypes: characterization, validation, and prognostic value. *PLoS Med.* 2013;10(5):e1001453.

19. Guinney J, Dienstmann R, Wang X, de Reynies A, Schlicker A, Soneson C, et al. The consensus molecular subtypes of colorectal cancer. *Nat Med.* 2015;21(11):1350-6.

20. Font-Clos F, Zapperi S, and La Porta CAM. Integrative analysis of pathway deregulation in obesity. *NPJ Syst Biol Appl.* 2017;3:18.

21. Ribeiro R, Monteiro C, Catalan V, Hu P, Cunha V, Rodriguez A, et al. Obesity and prostate cancer: gene expression signature of human periprostatic adipose tissue. *BMC Med.* 2012;10:108.

22. Creighton CJ, Sada YH, Zhang Y, Tsimelzon A, Wong H, Dave B, et al. A gene transcription signature of obesity in breast cancer. *Breast Cancer Res Treat.* 2012;132(3):993-1000.

23. Slattery ML, Mullany LE, Sakoda L, Samowitz WS, Wolff RK, Stevens JR, et al. The NF-kappa B signalling pathway in colorectal cancer: associations between dysregulated gene and miRNA expression. *J Cancer Res Clin.* 2018;144(2):269-83.

24. Cancer Genome Atlas N. Comprehensive molecular characterization of human colon and rectal cancer. *Nature.* 2012;487(7407):330-7.

25. Mermel CH, Schumacher SE, Hill B, Meyerson ML, Beroukhim R, and Getz G. GISTIC2.0 facilitates sensitive and confident localization of the targets of focal somatic copy-number alteration in human cancers. *Genome Biol.* 2011;12(4).

26. Liu JF, Lichtenberg T, Hoadley KA, Poisson LM, Lazar AJ, Cherniack AD, et al. An Integrated TCGA Pan-Cancer Clinical Data Resource to Drive High-Quality Survival Outcome Analytics. *Cell.* 2018;173(2):400-+.